Journal of Visualized Experiments

A fluorescence fluctuation spectroscopy assay of protein-protein interactions at cell-cell contacts

--Manuscript Draft--

Article Type:	Invited Methods Article - JoVE Produced Video
Manuscript Number:	JoVE58582R2
Full Title:	A fluorescence fluctuation spectroscopy assay of protein-protein interactions at cell-cell contacts
Keywords:	Protein-protein interaction; fluorescence microscopy; fluorescence fluctuation spectroscopy; Fluorescence correlation spectroscopy; membrane protein; multimerization
Corresponding Author:	Salvatore Chiantia Universitat Potsdam Potsdam, Brandenburg GERMANY
Corresponding Author's Institution:	Universitat Potsdam
Corresponding Author E-Mail:	chiantia@gmail.com
Order of Authors:	Valentin Dunsing
	Salvatore Chiantia
Additional Information:	
Question	**Response**
Please indicate whether this article will be Standard Access or Open Access.	Standard Access (US$2,400)
Please indicate the **city, state/province, and country** where this article will be **filmed**. Please do not use abbreviations.	Potsdam Universitaet, Institut fuer Biochemie, Karl-Liebknecht-Str. 24-25, Haus 25, 14476 Potsdam-Golm, Germany

Dear Editor,

We are submitting the revised version of the manuscript entitled “A fluorescence fluctuation spectroscopy assay of protein-protein interactions at cell-cell contacts” by V. Dunsing and S. Chiantia, as an invited article to be published in JOVE.

We are pleasantly surprised by the detailed feedback given by the reviewers and we have accordingly modified the manuscript. We have included a version of the document with the changes highlighted in red.

I believe that this article will be of great interest to many of the readers of JOVE and hope that you and the reviewers will be satisfied with the modifications.

Best regards,

Salvatore Chiantia

Jun.-Prof. Dr. Salvatore Chiantia

TITLE:

A Fluorescence Fluctuation Spectroscopy Assay of Protein-Protein Interactions at Cell-Cell Contacts

AUTHORS & AFFILIATIONS:

Valentin Dunsing[1], Salvatore Chiantia[1]

[1] University of Potsdam, Institute for Biochemistry and Biology, Cell Membrane Biophysics Group, Karl-Liebknecht-Str. 24-25, 14476 Potsdam, Germany

Corresponding Author:

Salvatore Chiantia

chiantia@uni-potsdam.de

Tel: +49-331-977-5872

Email Address of Co-author:

Valentin Dunsing (dunsing@uni-potsdam.de)

KEYWORDS:

Protein-protein interactions, cell-cell interactions, cell-cell adhesion, fluorescence fluctuation spectroscopy, fluorescence correlation spectroscopy, number and brightness, N&B

SHORT ABSTRACT:

This protocol describes a fluorescence fluctuation spectroscopy-based approach to investigate interactions among proteins mediating cell-cell interactions, *i.e.* proteins localized in cell junctions, directly in living cells. We provide detailed guidelines on instrument calibration, data acquisition and analysis, including corrections to possible artefact sources.

LONG ABSTRACT:

A variety of biological processes involve cell-cell interactions, typically mediated by proteins that interact at the interface between neighboring cells. Of interest, only few assays are capable of specifically probing such interactions directly in living cells. Here, we present an assay to measure the binding of proteins expressed at the surfaces of neighboring cells, at cell-cell contacts. This assay consists of two steps: mixing of cells expressing the proteins of interest fused to fluorescent proteins followed by fluorescence fluctuation spectroscopy measurements at cell-cell contacts using a confocal laser scanning microscope. We demonstrate the feasibility of this assay in a biologically relevant context by measuring the interactions of the amyloid precursor-like protein 1 (APLP1) across cell-cell junctions. We provide detailed protocols on the data acquisition using fluorescence-based techniques (scanning fluorescence correlation spectroscopy, cross-correlation number and brightness analysis) and the required instrument calibrations. Further, we discuss critical steps in the data analysis and how to identify and correct external, spurious signal variations, such as those due to photobleaching or cell movement.

In general, the presented assay is applicable to any homo- or heterotypic protein-protein interaction at cell-cell contacts, between cells of the same or different types and can be implemented on a commercial confocal laser scanning microscope. An important requirement is the stability of the system, which needs to be sufficient to probe diffusive dynamics of the proteins of interest over several minutes.

INTRODUCTION:

Many biological processes occur at the sites of cell-cell interactions, *e.g.,* cell-cell adhesion[1–3], cell-cell fusion[4] and cellular recognition[5]. Such events are particularly important during the development of multicellular organisms and for cell-cell communication, *e.g.,* during immune responses. These processes are typically mediated by proteins that are localized at the surface, *i.e.,* at the plasma membrane (PM) of neighboring cells and undergo specific interactions at the cell-cell contact that are precisely regulated in space and time. In many cases, these interactions are direct homo- or heterotypic protein-protein "trans" interactions, but may also involve ions or ligands acting as extracellular linkers[1]. Although of fundamental importance, there is a lack of assays probing these specific protein-protein interactions directly in the native environment of living cells. Many methods either require cell disruption (*e.g.,* biochemical assays such as co-immunoprecipitation[6]), fixation (*e.g.,* some of the super-resolution optical microscopy techniques and electron microscopy of cell-cell contacts[7]), or are non-specific, *e.g.,* aggregation/ adhesion assays[8, 9]. To overcome this issue, fluorescence techniques have been implemented based on fluorescence resonance energy transfer (FRET)[10] or fluorescence complementation[11]. However, to achieve sufficiently small distances between fluorophores, these methods require fluorescent labels on the extracellular side of the proteins[10], potentially interfering with *trans* interactions.

Here, we present an alternative fluorescence-based assay for protein-protein interactions at cell-cell contacts. This approach combines fluorescence cross-correlation approaches (scanning fluorescence cross-correlation spectroscopy (sFCCS), cross-correlation number and brightness (ccN&B) and mixing of cells expressing a fusion construct of the protein of interest, *e.g.,* an adhesion receptor. The investigated receptors in the two interacting cells are labeled with two spectrally separated fluorescent proteins (FPs), from the intracellular side (see **Figure 1A**).

The employed methods are based on the statistical analysis of fluorescence fluctuations induced by the diffusive motion of fluorescent fusion proteins through the focal volume of a confocal laser scanning microscope. More in detail, the assay probes the co-diffusion of the proteins of interest in both neighboring PMs at cell-cell contacts. If the proteins undergo *trans* interactions, these *trans* complexes will carry fluorescent proteins emitting in both spectral channels, causing correlated fluorescence fluctuations of both emitters. On the other hand, if no binding occurs, the number fluctuations of proteins in facing PMs will be independent, causing no correlated fluctuations. The acquisition can be performed in two ways: 1) sFCCS is based on a line-shaped scan across the cell-cell contact and effectively probes the interactions in a spot located in the contact region. Through a temporal analysis of fluorescence fluctuations, sFCCS provides also dynamics information, *i.e.* the diffusion coefficients of protein complexes; 2) ccN&B is based on a pixel-wise analysis of a sequence of images acquired at the cell-cell contact regions. It has

capability to probe and map interactions along the whole contact region (in one focal plane), but does not provide information on dynamics. Both methods can be combined with an analysis of the molecular brightness, *i.e.* the average fluorescence signal emitted in unit time by single diffusing protein complexes and, thus, provide estimates of the stoichiometry of protein complexes at the cell-cell contact.

In this article, we provide detailed protocols for sample preparation, instrument calibration, data acquisition and analysis to perform the presented assay on a commercial confocal laser scanning microscope. The experiments can be performed on any instrument equipped with photon counting or analog detectors and an objective with high numerical aperture. We further discuss critical steps of the protocol and provide correction schemes for several processes causing artefactual signal fluctuations, *e.g.,* detector noise, photobleaching or cell movement. Originally developed to probe interactions between adherent cells, the assay may be modified for suspension cells, or adapted to model membrane systems, *e.g.,* giant unilamellar vesicles (GUVs) or giant plasma membrane vesicles (GPMVs), allowing the quantification of interactions in different lipid environments or in the absence of an organized cytoskeleton[12, 13].

Scanning fluorescence cross-correlation spectroscopy is a modified version of fluorescence cross-correlation spectroscopy[14] and was specifically designed to probe slow diffusive dynamics in lipid membranes[15]. It is based on a line scan acquisition perpendicular to the PM containing the fluorescent proteins of interest. To probe interactions of two differently labeled protein species, the acquisition is performed in two spectral channels using two laser lines and two detection windows for the spectrally separated fluorophores. Due to the slow diffusion dynamics of proteins in the PM ($D \leq \sim 1\ \mu m^2/s$), a cross-talk-free measurement can be performed by alternating the excitation scheme from line to line[15]. The analysis starts with: 1) an alignment algorithm correcting for lateral cell movement based on block-wise averaging of ~1000 lines, 2) determination of the position with maximum fluorescence signal*, i.e.,* the PM position, in each block and 3) shifting of all blocks to a common origin[12, 15], separately in each channel. Then, an automatic selection of pixels corresponding to the PM is performed by selecting the central pixels of a Gaussian fit of the sum of all aligned lines (*i.e.* center ± 2.5 σ). Integration of the signal in each line yields the membrane fluorescence time series *F(t)* in each channel (g = green channel, r = red channel). Note that the pixel size has to be small enough, *e.g.,* <200 nm, to reconstruct the shape of the point spread function and find its center, corresponding to the position of the PM. In the presence of substantial photobleaching, the fluorescence time series in each channel may be fitted with a double-exponential function $f(t)$ and then corrected with the following formula[16]:

$$F(t)^c = \frac{F(t)}{\sqrt{f(t)/f(0)}} + f(0)\left(1 - \sqrt{f(t)/(f(0))}\right). \quad (1)$$

It is important to note that this formula effectively corrects both the amplitudes and diffusion times obtained from correlation analysis of $F(t)^c$, compared to parameter estimates that would be obtained from the uncorrected *F(t)*. Then, the auto- and cross-correlation functions (ACFs/ CCFs) of the fluorescence signals are calculated:

$$G_{auto}(\tau) = \frac{\langle \delta F_i(t) \delta F_i(t+\tau) \rangle}{\langle F_i(t) \rangle^2} \quad (2)$$

$$G_{cross}(\tau) = \frac{\langle \delta F_g(t) \delta F_r(t+\tau) \rangle}{\langle F_g(t) \rangle \langle F_r(t) \rangle} \quad (3)$$

where $\delta F_i = F_i(t) - \langle F_i(t) \rangle$ and $i = g, r$.

A two-dimensional diffusion model is then fitted to all correlation functions (CFs):

$$G(\tau) = \frac{1}{N}\left(1 + \frac{\tau}{\tau_d}\right)^{-1/2}\left(1 + \frac{\tau}{\tau_d S^2}\right)^{-1/2}. \quad (4)$$

Here, *N* denotes the number of fluorescent proteins in the observation volume and τ_d the diffusion time for each channel. This model takes into account that in the described experimental setting, diffusion of proteins in the PM occurs in the x-z plane, in contrast to the commonly used configuration of fluorescence correlation spectroscopy (FCS) experiments on membranes probing diffusion in the x-y plane of the confocal volume[17]. The waist w_0 and the structure factor S, describing the elongation w_z of the focal volume in z, $S = w_z/w_0$, are obtained from a point FCS calibration measurement performed with spectrally similar dyes and same optical settings using already available values for the diffusion coefficient D_{dye}:

$$w_0 = \sqrt{4\tau_{d,dye} D_{dye}}, \quad (5)$$

where $\tau_{d,dye}$ is the measured average diffusion time of the dye molecules, obtained from fitting a model for three-dimensional diffusion to the data, taking into account transitions of a fraction *T* of all *N* molecules to a triplet state with a time constant τ_T:

$$G(\tau) = \frac{1}{N}\left(1 + \frac{T}{1-T} e^{-\frac{\tau}{\tau_T}}\right)\left(1 + \frac{\tau}{\tau_{d,dye}}\right)^{-1}\left(1 + \frac{\tau}{\tau_{d,dye} S^2}\right)^{-1/2}. \quad (6)$$

Finally, diffusion coefficients (*D*), molecular brightness values (ε) and the relative cross-correlation of sFCCS data (*rel.cc.*) are calculated as follows:

$$D = {\omega_0}^2 / 4\tau_d \quad (7)$$

$$\varepsilon = \frac{\langle F(t) \rangle}{N} \quad (8)$$

$$rel.cc. = max\left\{\frac{G_{cross}(0)}{G^g_{auto}(0)}, \frac{G_{cross}(0)}{G^r_{auto}(0)}\right\}, \quad (9)$$

where $G_{cross}(0)$ is the amplitude of the cross-correlation function and $G^i_{auto}(0)$ is the amplitude of the autocorrelation function in the *i*-th channel.

This definition of the relative cross-correlation, *i.e.* using *max* instead of *mean* in Equation 9, takes into account that the maximum number of complexes of two protein species present at different concentrations is limited by the species present in a lower number.

Cross-correlation number and brightness is based on a moment analysis of the fluorescence intensity for each pixel of an image stack acquired over time at a fixed position in the sample, typically consisting of ~100–200 frames, with two spectral channels (g = green channel, r = red

channel). From the temporal mean $\langle I \rangle_i$ and variance σ_i^2, the molecular brightness ε_i and number n_i are calculated in each pixel and spectral channel ($i = g, r$)[18]:

$$\varepsilon_i = \frac{\sigma_i^2}{\langle I \rangle_i} - 1 \quad (10)$$

$$n_i = \frac{\langle I \rangle_i^2}{\sigma_i^2 - \langle I \rangle_i} . \quad (11)$$

It is important to note that the given equations apply to the ideal case of a true photon-counting detector. For analog detection systems, the following equations apply[19, 20]:

$$\varepsilon_i = \frac{\sigma_i^2 - \sigma_0^2}{S(\langle I \rangle_i - offset)} - 1 \quad (12)$$

$$n_i = \frac{(\langle I \rangle - offset)_i^2}{\sigma_i^2 - \sigma_0^2 - S(\langle I \rangle_i - offset)} . \quad (13)$$

Here, S is the conversion factor between detected photons and the recorded digital counts, σ_0^2 is the readout noise and *offset* refers to the detector intensity offset. Generally, these quantities should be calibrated, for any detector type, based on measuring the detector variance as a function of intensity for steady illumination[19], *e.g.,* a reflective metal surface or dried dye solution. The *offset* can be determined by measuring the count rate for a sample without excitation light. By performing a linear regression of the detector-associated variance σ_d^2 versus intensity $\langle I \rangle$ plot, S and σ_0^2 can be determined[19]:

$$\sigma_d^2 = S\langle I \rangle - S \cdot offset + \sigma_0^2 . \quad (14)$$

Finally, the cross-correlation brightness is calculated in each pixel and is defined in general as[21]:

$$B_{cc} = \frac{\sigma_{cc}^2}{\sqrt{\langle I_g \rangle \langle I_r \rangle}} , \quad (15)$$

where σ_{cc}^2 is the cross-variance $\sigma_{cc}^2 = \langle (I_g - \langle I_g \rangle)(I_r - \langle I_r \rangle) \rangle$.

In order to filter long-lived fluctuations, all ccN&B calculations are performed following a boxcar filtering, independently for each pixel[22]. Briefly, n_i, ε_i ($i = g, r$) and B_{cc} are calculated in sliding segments of *e.g.,* 8–15 frames. The values thus obtained can be then averaged to obtain the final pixel number and brightness values.

Stoichiometry analysis

In order to estimate the stoichiometry of protein complexes at cell-cell contacts, the molecular brightness can be separately analyzed in each spectral channel for the sFCCS or ccN&B data. In sFCCS, one brightness value is obtained per measurement in each channel. In ccN&B, a brightness histogram of all pixels corresponding to the cell-cell contact is obtained and the average (or median) value can be used as representative brightness for the measurement. By performing the same analysis on a monomeric reference, all brightness values can be normalized to directly obtain the average oligomeric state of the detected protein complexes. At this point, it is important to correct for the presence of non-fluorescent FPs that may result in an underestimation of the oligomeric state. This is typically performed by measuring the brightness of a homo-dimeric reference protein[23, 24] using one-color sFCS or number and brightness (N&B).

PROTOCOL:

1. Sample Preparation: Cell-Cell Mixing Assay

Note: The following protocol describes the mixing procedure for adherent cells. It may be modified for cells cultured in suspension.

1.1. Seed an appropriate number of cells on a 6-well plate, *e.g.,* 800,000 HEK 293T cells (counted with a Neubauer counting chamber), a day before transfection. The number can be modified depending on the time between seeding and transfection and adjusted for other cell types. To perform a basic experiment (*i.e.* proteins of interest and negative control), prepare at least 4 wells. Culture cells at 37 °C, 5% CO_2 in Dulbecco's Modified Eagle Medium (DMEM) medium, supplemented with fetal bovine serum (10%) and L-glutamine (1%).

1.2. Transfect cells according to the manufacturer's instructions (see the **Table of Materials**).

1.2.1. To perform a basic experiment, transfect, in separate wells, plasmids for the protein of interest fused to a 'green' (*e.g.* monomeric enhanced green (mEGFP), yellow fluorescent protein (mEYFP)) or 'red' (*e.g.* mCherry, mCardinal) fluorescent protein.

Note: In this protocol, we focus on APLP1-mEYFP and APLP1-mCardinal[12], and the corresponding negative control, *e.g.* myristoylated-palmitoylated-mEYFP (myr-palm-mEYFP) and -mCardinal (myr-palm-mCardinal)[12]. Generally, 200 ng – 1 µg of plasmid DNA are sufficient. High transfection efficiency increases the chance to find red and green cells in contact. Modify the amount of plasmid and transfection reagent to optimize transfection efficiency. **Critical:** Cell confluency should be around 70% when transfecting the cells. If cells are over-confluent, the transfection efficiency will decrease. If cells are not confluent enough, transfection and mixing may induce stress and prevent many cells from proper attachment after mixing.

1.3. Perform cell mixing ~4 ± 2 h after transfection.

1.3.1. Remove growth medium and wash each well gently with 1 mL PBS supplemented with Mg^{2+} and Ca^{2+}. Then, remove the PBS. (**Critical**) Drop PBS on well edge to prevent detachment of cells during washing.

1.3.2. Add ~50 µL trypsin ethylenediaminetetraacetic acid (EDTA) solution drop-wise to each well to facilitate detachment of cells. Incubate at 37 °C for 2 min. Afterwards, slowly shake the 6-well plate laterally to detach the cells.

Note: Extended incubation times may be required for some cell types.

1.3.3. Add 950 µL of growth medium to each well and resuspend cells by pipetting a few times up and down, thereby detaching all cells from the well bottom. (**Critical**) Ensure that cells are resuspended properly and detached from each other by visually checking for the absence of large

cell aggregates after resuspension. Otherwise many 'red'-'red' or 'green'-'green' contacts will be obtained after mixing.

1.3.4. Transfer the cell solution of one well (protein of interest or negative control) to the corresponding well, *i.e.,* 'red' (*e.g.* APLP1-mCardinal transfected) to 'green' (*e.g.* APLP1-mEYFP transfected) cells. Mix by gently pipetting a few times up and down. Then, seed the mixed cells on 35-mm glass bottom dishes (1 mL of mixed cell solution per dish, plus 1 mL of growth medium) and culture seeded cells for another day at 37 °C, 5% CO_2.

[Place Figure 1 here]

2. Sample Preparation: Positive Control for Cross-Correlation Experiments and Homo-Dimer Construct for Brightness Analysis

2.1. Seed 600,000 HEK 293T cells, counted with a cell counting chamber, on 35-mm glass bottom dishes one day before transfection. Culture the cells at 37 °C, 5% CO_2 in complete DMEM medium (see step 1.1) for another day.

2.2. Transfect cells with ~250 ng of plasmid DNA according to manufacturer instructions. For the positive cross-correlation control, use a plasmid encoding a membrane-anchored fluorescent protein hetero-dimer, *e.g.,* myr-palm-mCherry-mEGFP or myr-palm-mCardinal-mEYFP[12] corresponding to the FPs of the protein of interest. For brightness calibration, use plasmids encoding both a membrane-anchored FP monomer and homo-dimer corresponding to the FPs fused to the protein of interest , *e.g.,* myr-palm-mEYFP and myr-palm-mEYFP-mEYFP to calibrate brightness analysis of APLP1-mEYFP[12].

2.3. Culture cells at 37 °C, 5% CO_2 in complete DMEM medium (see step 1.1) for another day**.**

3. Confocal Laser Scanning Microscopy: Setup and Focal Volume Calibration

Note: The following protocol is written for experiments performed with mEGFP/mEYFP and or mCherry/mCardinal on the laser scanning confocal microscope used in this study. The optical setup, the software settings (laser lines, dichroic mirrors, filters) and choice of calibration dyes may be modified for other FPs and microscope setups.

3.1. Turn on the microscope and lasers at least an hour before the experiment to ensure laser stability and equilibration of temperature.

3.2. Prepare 100–200 µL of appropriate water-soluble fluorescent dye solutions (see the **Table of Materials** for examples) in water or PBS to calibrate the focal volume, with concentrations in the 10-50 nM range.

3.3. Place the dye solutions on a clean 35-mm glass bottom dish #1.5, *i.e.* having a thickness of 0.16–0.19 mm.

Note: Ideally, use dishes with high performance cover glass having a low thickness tolerance, *e.g.,* 0.170 ± 0.005 mm, allowing an optimal collar ring correction (step 3.6). It is important to use the same type of dish as used later for the following experiments.

3.4. Place the dish containing the dye solution directly on the objective (preferably, water immersion, with NA 1.2) to ensure focusing into the solution. Alternatively, place the dish on the sample holder and focus into the sample (*e.g.,* 10–20 µm above the bottom of the dish).

Note: We do not recommend using oil objectives due to the poor signal obtained when focusing deep into aqueous samples.

3.5. Set up the excitation and emission path, *e.g.,* choose the 488 nm laser, a 488/561 nm dichroic mirror, detection window 499–552 nm and a pinhole size of 1 Airy unit (AU). Make sure that the pinhole size is the same as that will be used in cross-correlation measurements.

3.6. Adjust pinhole position (**pinhole adjustment**) and the objective collar ring to maximize count rate. To this aim, turn collar ring until maximum count rate is detected.

Note: The collar ring correction accounts for the specific thickness of the cover glass used. Maximizing the count rate, *i.e*. collecting as many photons per molecule as possible, is crucial to maximize the signal-to-noise ratio (SNR) of the measurements.

3.7. Perform a series of point FCS measurements (*e.g.,* 6 measurements at different locations, each consisting of 15 repetitions of 10 s*, i.e.* 2.5 min total time, sampled with 1 µs dwell time or less) at the same laser power as used in cross-correlation measurements (typically ~1%, *i.e.,* ~1–2 µW).

3.8. Fit a three-dimensional diffusion model including a triplet contribution (Equation 6) to the data.

Note: Typically, the obtained diffusion times are around 30 µs and the structure factor is around 4–8.

3.9. Calculate the waist w_0 from the measured average diffusion time and published values for the diffusion coefficient of the used dye at room temperature[25] according to Equation 5. Typical values are 200–250 nm.

3.10. Repeat the calibration routine (steps 3.4–3.9) with a different fluorescent dye for a second detection channel if needed (*e.g.,* 561 nm excitation and detection between 570 nm and 695 nm). Keep the pinhole position and size as it was set for the first detection channel.

3.11. Calculate the molecular brightness (Equation 8) from the calibration measurements, and store the obtained values.

Note: Typical values for the used setup are ~8–10 kHz/molecule (MOL) for 1.8 µW 488 nm excitation power. Lower than usual values might indicate dirt on the objective, misalignment of the setup or a reduced laser output. Check and store laser output powers at the objective regularly using a power meter. For comparison of different setups, molecular brightness normalized by the excitation laser power is the most meaningful parameter to assess microscope performance.

4. Scanning Fluorescence Cross-Correlation Spectroscopy: Acquisition

Note: The following protocol is written for experiments performed with mEGFP/mEYFP ('green') and or mCherry/mCardinal ('red') on the laser scanning confocal microscope used in this study. The optical setup and the software settings (laser lines, dichroic mirrors, filters) may be different for other FPs or microscopy setups.

4.1. Set up the optical path, *e.g.,* 488 nm and 561 nm excitation and a 488/561 nm dichroic mirror, pinhole on 1 AU for 488 nm excitation. To avoid spectral cross-talk, select two separate tracks to excite and detect mEGFP/mEYFP (488 nm excitation, green channel) and mCherry/ mCardinal (561 nm excitation, red channel) sequentially and select **switch tracks every line**. For the detection, use appropriate filters for both channels, *e.g.,* 499–552 nm in the green channel and 570–695 nm in the red channel.

4.2. If alternated excitation is not possible, use appropriate filter settings for the red channel to minimize spectral cross-talk (*i.e.* detect mCherry/mCardinal fluorescence not below 600 nm). This may reduce the amount of photons detected in the red channel and thus reduce the SNR.

4.3. Place the dish containing the mixed cells on the sample holder. Wait at least 10 min to ensure temperature equilibration and to reduce focus drift.

4.4. Focus on the cells using transmission light in the **Locate** menu.

4.5. Search for a pair of 1 'red' and 1 'green' cells in contact with each other. For the positive cross-correlation or homo-dimer brightness control (see section 2), search for an isolated cell emitting fluorescence in both channels or the respective homo-dimer signal at the PM.

Note: **(Critical)** Minimize exposure of the cells while searching for cells to avoid pre-bleaching, which may reduce the cross-correlation[26]. Therefore, scan at the fastest scan speed and low laser powers. To avoid detector saturation while imaging strongly expressing cells, search in **integration mode**. However, to minimize exposure, scanning at lower laser powers is possible in **photon counting** mode.

4.6. Select a scan path perpendicular to cell-cell contact (or to PM of a single cell for the positive cross-correlation or homo-dimer brightness control) using the **Crop** button as depicted in **Figures 1B** and **2A**.

Note: Some older microscopes do not allow arbitrary scan directions. In this case, cell-cell contacts with an orientation perpendicular to the scan direction have to be located.

4.7. **Zoom** to achieve a pixel size of 50–200 nm and select **Line** in **Scan Mode**. Set **Frame Size** to 128 × 1 pixels.

Note: Typical pixel size is 160 nm, corresponding to a scan length of around 20 µm.

4.8. Set **Scan speed** to the maximum allowed value, *e.g.,* 472.73 µs per line.

Note: For an alternate excitation scheme, this corresponds to 954.45 µs scan time, *i.e.* ~1000 scans/s on the setup used. The scan speed may be adjusted depending on the diffusion coefficient of the protein of interest. For membrane-anchored proteins, typical diffusion times are around 10–20 ms. The scan time should be at least ten times smaller than the diffusion times. Lower scan speeds may induce stronger photobleaching and require lower illumination powers. Alternatively, one can impose a pause, *e.g.,* 5 ms, in between each scan for very slowly diffusing complexes using **Interval** in the **Time Series** submenu.

4.9. Choose the appropriate laser powers, *e.g.,* ~1-2 µW for 488 nm and ~5-10 µW for 561 nm excitation.

Note: Higher laser powers improve SNR, but increase photobleaching. Therefore, laser powers should be chosen such that photobleaching is less than 50% of the initial count rate.

4.10. Set **Cycles** to 100,000–500,000.

Note: The number of scans, *i.e.* duration of the measurement, may vary: Longer measurement times will improve SNR and may be more appropriate for slowly diffusing molecules, however, motion of the cells and photobleaching limit the maximal measurement time. Data presented here were routinely acquired for ~3–6 min, *i.e.* 200,000–400,000 line scans.

4.11. Set detectors to **Photon counting** mode. Press **Start Experiment** to start the acquisition. Repeat steps 4.5–4.11 to measure another cell.

Note: It is recommended to measure 10–15 cells per sample at different expression levels. (**Critical**) Avoid detector saturation at high expression levels. The maximum count rate should not exceed ~1 MHz.

4.12. If brightness analysis is carried out to determine oligomeric states, perform homo-dimer brightness calibration measurements according to modified steps 4.1–4.11: Measure each fluorescent protein homo-dimer separately (in isolated cells, prepared using protocol section 2) and perform measurements only in one spectral channel.

5. Scanning Fluorescence Cross-Correlation Spectroscopy: Data Analysis

Note: The following protocol follows an implementation of the analysis procedure described in detail in previous articles[12, 15]. The software code is available upon request to the authors.

5.1. Export the raw data (*e.g.,* CZI) files to an RGB TIFF image in raw data format. This file will contain a kymograph with the green and red channel data, in the channel termed G and R of the image, respectively.

5.2. Import the TIFF file with the appropriate analysis software and proceed to perform the analysis.

Note: The following steps (steps 5.3–5.7) are applied separately to each channel:

5.3. Align the lines by performing a segment-wise or moving time average with blocks of 500–1000 lines. Determine the membrane position, *i.e.* the pixel position with the maximum count rate, in each block. Shift all blocks to the same lateral position. This procedure corrects for lateral displacement of the cell-cell contact, *e.g.,* due to cell movement.

5.4. Sum up all aligned lines along the time axis and fit the average intensity profile using a Gaussian function. In the presence of significant intracellular background, use a Gaussian plus a sigmoid function. Define the pixels corresponding to the membrane as all pixels within $\pm 2.5\sigma$ of the membrane position and sum up the intensity of these pixels in each line, obtaining a single fluorescence signal value for each time point (*i.e.* for each line scan).

5.5. If needed (*e.g.,* background >10% of the sample signal), apply a background correction by subtracting the average pixel intensity in the cytoplasm multiplied by 2.5σ (in pixel units) from the membrane fluorescence, in blocks of 1000 lines. Avoid bright intracellular vesicles when selecting background pixels.

5.6. If photobleaching is observed, apply a bleaching correction. For this, fit the membrane fluorescence time series with a double-exponential function and apply the appropriate correction formula, Equation 1[16].

Note: Alternatively, Fourier spectrum based correction schemes may be applied[27]. (**Critical**) If photobleaching is present but not corrected for, the CFs may be severely distorted and parameter estimates may be strongly biased (*e.g.*, see **Figure 5E**).

5.7. Calculate the ACFs and CCFs according to Equations 2 and 3 using *e.g.,* a multiple-tau algorithm[28]. To improve the reliability of the analysis and avoid artefacts, perform the calculations for 10–20 equal segments of the total measurement. Inspect the fluorescence time series and CFs in each segment and remove clearly distorted segments (see examples in **Figures 4A–4D**). Average all non-distorted segments.

Note: This procedure can be automated to avoid a subjective bias to the data[29]. For very unstable measurements, many short segments may be helpful. However, the length of a segment should still be at least three orders of magnitude above the diffusion time to avoid statistical undersampling errors[29, 30, 17].

5.8. Fit a two-dimensional diffusion model, Equation 4, to the obtained CFs. Therefore, fix the structure factor to the value obtained in calibration measurement (Protocol section 3). The accuracy of the fit can be improved by performing a weighted fit using the statistical weights of each data point obtained from the multiple tau algorithm.

5.9. Calculate the diffusion coefficient using the calibrated waist according to Equation 7.

5.10. Calculate the molecular brightness by dividing the average fluorescence intensity in each channel by the corresponding number of particles, Equation 8. Normalize the determined brightness value in each channel by the average brightness of the corresponding monomeric reference to obtain the oligomeric state, taking into account non-fluorescent FPs[23]. To this aim, determine average homo-dimer brightness values from one-color analysis to calculate the fraction of non-fluorescent FPs[23].

5.11. Calculate the relative cross-correlation according to Equation 9.

6. Cross-Correlation Number and Brightness: Detector Calibration

Note: The following protocol provides a general guideline regarding how to calibrate the detection system. This procedure is mandatory for analog detection systems, but is not strictly needed when true photon counting detectors are used.

6.1. Dry appropriate water-soluble dye solutions (see **Table of Materials** for examples) on a 35-mm glass bottom dish. Set the optical path accordingly, *i.e.* 488 or 561 nm excitation and detection at 499–552 nm or 570–695 nm, respectively.

Note: Alternatively, a reflective metal surface can be used instead of dried dye solutions by placing the metal piece directly on top of the objective.

6.2. Perform one-color N&B measurements in regions with different dye concentrations or at different laser powers. Therefore, use **Zoom** to achieve a pixel size of 300 nm, **Scan speed** to set appropriate pixel dwell time, *e.g.,* 25 µs and set **Cycles** to 100–200 frames.

6.3. Set detectors to **photon counting** (or **analog mode** if measurements are performed with analog detection) and press **Start Experiment** to start the acquisition. Perform measurement at zero excitation power to determine the intensity offset.

6.4. Plot pixel variance as a function of pixel intensity for all measured pixels and perform a linear fit of these data. Determine S as the slope of the linear fit. Calculate the readout noise from the y-intercept, using S and the determined intensity offset according to Equation 14.

7. Cross-Correlation Number and Brightness: Acquisition

7.1. Follow steps 4.1–4.4 of the sFCCS acquisition protocol.

7.2. Use **Crop** to select a frame of 512 × 128 pixels around a cell-cell contact (or isolated PM for homo-dimer brightness control) and **Zoom** to achieve a pixel size of 50–100 nm.

7.3. Use **Scan speed** to set appropriate pixel dwell time, *e.g.,* 6.3 µs.

Note: In N&B, the pixel dwell time should be much smaller than the diffusion time of the protein of interest. If an alternate excitation scheme is chosen, *e.g.,* switching tracks every line, the time between the two tracks should be smaller than the diffusion time of the protein of interest. Otherwise the detectable cross-correlation is reduced.

7.4. Set **Cycles** to 100–200 frames.

Note: A higher frame number will improve the SNR, however, cell movement may limit the total measurement time. The scan time per frame should be much higher than the diffusion time of the protein of interest. Otherwise the apparent brightness is reduced, *i.e.* particles appear to be immobile. For very slowly diffusion complexes, impose a pause, *e.g.,* 2 s, in between frames using *Interval* in the *Time Series* submenu.

7.5. Set laser power to appropriate value (typical values are ~1–2 µW for 488 nm and ~5–10 µW for 561 nm excitation).

Note: Higher laser power leads to higher brightness and improved SNR, but also enhanced photobleaching. Laser powers should be high enough to achieve a detected brightness of at least ~1 kHz/MOL but kept low enough to avoid more than 10–20% photobleaching. For mEGFP/mEYFP or mCherry/mCardinal, less than 10% photobleaching are usually obtained.

7.6. Set detectors to **photon counting** (or **analog mode** if measurements are performed with analog detection). Press **Start Experiment** to start the acquisition.

7.7. Evaluate the photon count rate. If count rates in cell-cell contact pixels exceed 1 MHz, reduce the laser power or select cells with lower expression levels. Repeat the steps 7.2–7.7. to measure the next pair of cells. It is recommended to measure 10-15 cells per experiment at different expression levels.

7.8. If brightness analysis is performed to quantify oligomerization, perform homo-dimer brightness calibration measurements according to modified steps 7.1–7.7: Measure each

fluorescent protein homo-dimer separately (in isolated cells, prepared using protocol section 2) and perform measurements only in one spectral channel.

8. Cross-correlation Number and Brightness: Data Analysis

Note: The following protocol follows a previously described analysis procedure[12, 31]. The software code is available from the authors upon request.

8.1. Import the raw data (*e.g.,* CZI files can be imported using the Bioformats[32] package). Average all frames and select a region of interest (ROI) around the cell-cell contact

8.2. Perform an image alignment algorithm[33], *e.g.,* by maximizing the spatial correlation between ROIs in subsequent frames for arbitrary lateral translations, averaged over both channels. This procedure will correct for lateral movement of the cells.

8.3. Apply a boxcar filter[22] to reduce extraneous long-lived fluctuations, originating from *e.g.,* residual cell movement or background bleaching. Alternatively, an exponential detrending method may be applied to correct for photobleaching[34].

Note: If no segment-wise analysis or detrending is applied, the apparent brightness may be largely overestimated.

8.3.1. Define sliding segments of *e.g.,* 8 to 15 frames (*e.g.,* frames 1 to 8, 2 to 9 and so forth) and calculate the channel and cross-correlation brightness values according to Equations 10, 11 and 15 pixel-wise in each segment. If detectors are not true photon counting detectors, take the calibrated detector parameters into account when calculating the brightness, *i.e.* use Equations 12 and 13 instead.

Note: Calculating the brightness values in segments of 8 to 15 frames leads to a 10–20% underestimation of the absolute brightness and a 10–20% overestimation of particle numbers. Nevertheless, brightness ratios (*e.g.,* dimer to monomer brightness) are not affected, as long as the segment length is kept constant throughout the analysis (data not shown). The statistical error for a given segment length can be determined via simulations and thus corrected for.

8.3.2. Average the obtained brightness values pixel-wise over all segments. In this step, one may remove the highest and lowest 5% of segment brightness values from the average or exclude segments which show a clear distortion in the intensity, due to *e.g.,* an intracellular vesicle or aggregate transiently present in these pixels.

8.4. Plot the pixel brightness values as a function of the pixel intensity and select the population of pixels that corresponds to the cell-cell contact. Background pixels will have very low intensity values. At this point, re-evaluate the maximum count rate. Exclude pixels with count rates above 1 MHz to prevent pile-up effects.

8.5. Create channel and cross-correlation brightness histograms of selected cell-cell contact pixels and fit with a Gaussian function to obtain the ROI-averaged brightness values. Normalize the average channel brightness value by the average brightness of the corresponding monomeric reference to obtain the oligomeric state, taking into account non-fluorescent FPs[23]. Therefore, determine average homo-dimer brightness values from one-color analysis to calculate the fraction of non-fluorescent FPs[23].

8.6. For illustration, plot channel and cross-correlation brightness maps.

REPRESENTATIVE RESULTS:

A first test for the protein-protein interaction assay, *i.e.* mixing of cells expressing spectrally distinct fluorescent proteins followed by sFCCS/ccN&B measurements (**Figure 1**), should be performed on proteins that are not expected to interact at the cell-cell contact (*i.e.* a negative control). Therefore, HEK 293T cells expressing myristoylated-palmitoylated-mEYFP (myr-palm-mEYFP) or -mCardinal were mixed and sFCCS was performed across the cell-cell contact (**Figure 2A).** In an ideal case, the fluorescence signal in each channel is supposed to fluctuate around a stable mean, as a consequence of the diffusive motion of the proteins in the PM and the statistical variations of the number of proteins in the focal volume. For proteins that do not interact, the fluctuations in both channels are independent from each other and, thus, the spectral cross-correlation is expected to fluctuate around zero. Indeed, a relative cross-correlation close to zero was observed in typical measurements (**Figure 2C**), while the ACFs show characteristic decay times of ~10–20 ms (corresponding to, on average, $D_{myr\text{-}palm}$ = 1.3 ± 0.3 µm^2/s (mean ± SD), n = 20 cells) as expected for the diffusion of myr-palm-mEYFP and -mCardinal in the PM, *e.g.,* $D_{myr\text{-}palm}$ = 0.88 ± 0.11 µm^2/s (mean ± SEM) based on fluorescence recovery after photobleaching (FRAP) experiments[35]. Notably, these rather slow dynamics allow the use of an alternating excitation scheme, *i.e.* switching between only green and only red excitation and detection every line, causing a ~0.5 ms delay between signals in both channels but suppressing spectral cross-talk. On average, a very low average cross-correlation of 0.08 ± 0.10 (mean ± SD, n = 17 cells) was obtained for the negative control (**Figure 3E**), as expected.

Next, a positive cross-correlation control was used to calibrate the maximum possible cross-correlation in the optical setup. Therefore, the membrane-anchored hetero-dimer myr-palm-mCardinal-mEYFP was expressed in HEK 293T cells and sFCCS measurements were performed on single cells (**Figure 2B**). The obtained CCFs had positive amplitudes and showed similar decay times as the AFs, again ~10–20 ms (**Figure 2D**). On average, a relative cross-correlation of 0.96 ± 0.18 (mean ± SD, n = 14 cells) was measured for the positive control (**Figure 3E**).

[Place Figure 2 here]

The suitability of this assay was then investigated in a biologically relevant context by probing the *trans* interactions of the amyloid precursor-like protein 1 (APLP1), a type I transmembrane protein that has been proposed to act as a neuronal adhesion receptor. To this aim, APLP1 fused to mEYFP or mCardinal was expressed in HEK 293T cells. To exclude interference with extracellular binding domains, the FPs were fused to the C-terminus of APLP1, *i.e.* at the

intracellular domain (see **Figure 1A**). Then, sFCCS measurements were performed on cell-cell contacts between APLP1-mEYFP and APLP1-mCardinal expressing cells (**Figure 3A**), resulting in ACFs and CCFs (**Figure 3C**) that provide information about APLP1 diffusion and interactions. A positive relative cross-correlation of 0.45 ± 0.21 (mean ± SD), n = 17 cells) was observed, *i.e.* a value significantly larger than that of the negative control (**Figure 3E**). Interestingly, the average relative cross-correlation was lower than that of the positive control (**Figure 3E**), indicating only partial *trans* binding.

Finally, the assay was used to show that zinc ions facilitate enhanced APLP1 *trans* binding[12, 31]. The sFCCS CFs obtained from measurements across APLP1 clusters at cell-cell contacts (characterized by a strong co-localization of APLP1-mEYFP and APLP1-mCardinal and forming rapidly in the presence of zinc ions, **Figure 3B**) showed strongly reduced dynamics, as evident from large decay times and the oscillations at large lag times (**Figure 3D**). Nevertheless, analysis of the amplitudes at short lag times revealed a significant increase of the relative cross-correlation to 0.8 ± 0.3 (mean ± SD, n = 17 cells), *i.e.* ~80% of the calibrated maximum (**Figure 3E**). It is to be expected that such slow dynamics induce severe distortions of the correlation curves (see **Figure 3D**) due the limited number of diffusive events that can be detected during the finite measurement time, inducing so-called particle noise[30]. For an accurate quantification, the maximum lag time should be at least 3 orders of magnitude above the diffusion time (see previous reviews[30, 17] for further details).

The molecular brightness from the sFCCS APLP1 data was further analyzed, using the myr-palm negative control as a monomeric reference in each channel and correcting for the amount of non-fluorescent proteins[23]. Upon zinc ion addition, the molecular brightness significantly increased from small oligomers (~dimers) to larger multimers consisting of ~10–50 monomers on each cell (**Figure 3F**). Thus, on average, up to ~100 APLP1 monomers are present in a whole protein cluster across the cell-cell junction.

[Place Figure 3 here]

All the measurements shown so far were corrected for additional, spurious fluctuations occurring in the cells that, if not taken into account, would make the sFCCS analysis challenging. For the negative control, for example, these may cause a false-positive cross-correlation, if no correction schemes are applied. Two major processes that can severely distort the CFs are: 1) instabilities in the recorded fluorescence signal due to intracellular vesicles that transiently enter the focal volume or slow membrane dynamics, *e.g.,* drift in the z-direction, and 2) photobleaching. To identify transient instabilities, it is recommended to analyze the full measurements in 10–20 equally sized segments and to visually inspect the intensity time series and CFs in each segment. This procedure is illustrated in **Figure 4**, which gives an example of clearly distorted segments obtained in the analysis of a negative control measurement. Transient instabilities (**Figure 4A**, intensity traces of segments 1 and 2) may result in a CCF having negative values (**Figure 4B**, segment 1) or a high false-positive cross-correlation (**Figure 4B**, segment 2). Typically, such instabilities are visible in the intensity series as slow signal variations (**Figure 4A**). The corresponding CFs typically deviate strongly from the CFs of the majority of segments, displaying

e.g., higher amplitude and much slower decay times on the ~second scale (see **Figures 4B–4D**). It is recommended to remove such segments from the analysis and to calculate the final CFs by averaging all non-distorted segments, *i.e.* segments characterized by CFs not deviating from the majority of CFs. Typically, this is done in a graphical interface by 1) iteratively examining the segments, 2) removing clearly distorted segments from the average and 3) inspecting the CFs of remaining segments with respect to the updated average CFs of segments that were not removed. By applying this procedure, partially distorted long measurements (**Figure 5A**), showing slowly decaying (corrupted) CFs (**Figure 5B**) were successfully corrected and meaningful correlation curves were recovered (**Figure 5C**). Generally, this correction procedure can be automatized[29], avoiding a visual inspection by the user, which may be prone to subjective bias. In comparison to intensity based filtering methods[36], in which small bins of the measurement are evaluated based on their intensity compared to the average intensity of the full measurement and removed if exceeding a threshold parameter, the described procedure does not rely on external parameters and is sensitive also to minor instabilities.

In order to compensate for photobleaching, the described mathematical correction, **Equation 1**, was applied. Typically, photobleaching can be identified by an exponential decay of the fluorescence signals (**Figure 5D)**, dominating the CFs, which then show a false-positive cross-correlation and decay times on the ~min scale (see the typical curve shape in **Figure 5E**). The correction procedure recovered the non-distorted CFs (**Figure 5F**). As already mentioned, similar intensity variations within single measurements may be also caused by PM movement, *e.g.,* z-drift, or large slowly moving structures. However, if similar exponential decays appear in all measurements, photobleaching will be the most likely source. Generally, correction schemes can be combined, *e.g.,* intensity filtering, CF based filtering and further methods such as Fourier transform based filtering of slow signal variations in frequency space[27].

[Place figures 4 and 5 here]

As a complementary approach to sFCCS, ccN&B (**Figure 1C**) can be used to detect protein-protein interactions after cell mixing. In contrast to sFCCS, ccN&B provides no information on protein dynamics, but allows measuring *trans* interactions along the whole cell-cell contact in one focal plane. Measurements on APLP1 samples were performed before and after treatment with 50 µM $ZnCl_2$, as well as on the negative myr-palm control. These measurements are sensitive to cell movements, especially for zinc ion treated samples, requiring prolonged acquisition times to account for the slow dynamics of APLP1 clusters. Therefore, an image alignment algorithm was implemented to correct for lateral movement of the cells[33]. Also, a boxcar filter[22] (8 frames box size, ~5 s) was applied to remove low frequency fluctuations of the measured signals. This procedure is very similar to other filters used in N&B analysis involving local averaging[37] or detrending[18, 34], but keeps the original data unaltered, *i.e.,* pixels are treated independently and no averaging or subtraction of signals is performed. This procedure effectively suppresses long-lived fluctuations on time scales longer than the box size[22]. Following such data analysis, the cross-correlation brightness values for all samples were compared by pooling all cell-cell contact pixels in a cross-correlation brightness histogram. For APLP1 in the absence of zinc ions (**Figures 6A** and **6D**), a positive average B_{cc} of 0.068 ± 0.004 (mean ± SEM, n = 18 cells) was observed. After

zinc ion addition (**Figure 6B** and **6E**), the B_{cc} value increased to 0.266 ± 0.006 (mean ± SEM, n = 19 cells). For the negative control (**Figure 6C** and **6F**), a lower average cross-correlation brightness was detected (B_{cc} =0.022 ± 0.002, mean ± SEM, n = 26 cells). To estimate the stoichiometry of APLP1 complexes at cell-cell contacts, the brightness of APLP1-mEYFP was normalized using the average value obtained for myr-palm-mEYFP (*i.e.*, the negative control) and corrected for the amount of non-fluorescent proteins[23]. In agreement with sFCCS data, the brightness distribution was centered around a value corresponding to dimers (**Figure 6G**), in the absence of zinc ions, suggesting an average 2:2 stoichiometry. After zinc ion treatment, the normalized brightness strongly shifted to larger values, ranging from ~10 to ~60 (**Figure 6H**), *i.e.*, stoichiometries of at least 10:10 or larger, again in good agreement with sFCCS data.

[Place figure 6 here]

In order to perform the ccN&B analysis, a careful calibration of the detectors should be performed. For the experimental setup used in this study, the need for such a calibration became apparent when the molecular brightness was analyzed in fixed samples (*i.e.,* in the absence of number fluctuations). In this case, the molecular brightness is expected to be zero according to Equation 10, since the variance should only originate from detector noise. However, when a ROI that contains only (immobile) background pixels was analyzed (**Figure 7A** and **7B**), a positive brightness of ~0.1 cts./(MOL·dwell time) was determined. A similar value was obtained performing N&B measurements of HEK 293T cells expressing glycosylphosphatidylinositol-mCherry (GPI-mCherry, **Figure 7C**) with varying laser powers and extrapolating the measured molecular brightness to zero laser power. To correct for this effect, we performed a systematic calibration of the detector, as previously reported (see Equation 12)[19, 20]. We therefore measured the variance as a function of detector count rate on a sample consisting of a dried fluorescent dye solution and determined the parameters S, σ_0^2 and the dark count rate offset. The latter was obtained from measuring the intensity at zero laser power and was, in our case, negligible. From a linear fit of the variance versus intensity plot, we determined, according to Equation 14, a slope of S = 1.1, and a negligible readout noise. The determined values (S = 1.1, σ_0^2 = 0, *offset* = 0) were then used to correctly calculate molecular brightness and number according to Equations 12 and 13[19]. Alternatively, a more empirical correction scheme can be applied based on the fact that a superpoissonian detector noise, *i.e.* ~10% larger noise than Poissonian shot noise, would also explain the observation of a positive molecular brightness in pixels without number fluctuations. Using this assumption, the determined brightness of ~0.1 cts./(MOL·dwell time) in such pixels can be considered as a constant brightness offset and should thus be subtracted from all brightness values calculated with Equation 10. Most importantly, both described approaches lead to the same results when calculating brightness ratios, as long as σ_0^2 and *offset* are negligible. It is worth mentioning that among different microscopes of the same type (same vendor, same model, GaAsP detectors in photon counting mode) different S values were observed, highlighting the necessity for a careful detector calibration on each individual setup.

A further important parameter affecting the detector performance in brightness measurements is the detector dead time. As it has been previously shown, the detector dead time can substantially reduce the detected molecular brightness, even at medium count rates (above 10^2–

10^3 kHz)[38]. To avoid this artefact, measurements should either be performed at lower count rates, or the dead time should be calibrated based on performing N&B or FCS in a dilution series of *e.g.,* EGFP in buffer solution. Then, measured count rates can be corrected using a calibrated dead time[38]. For the setup used in this study, such a calibration using N&B on diluted dye solutions revealed stable molecular brightness values up to count rates of ~0.5 MHz and a corresponding dead time of ~6 ns (**Figure 7E**). The decrease at higher count rates can be thus corrected by using a previously published correction formula[38], resulting in a constant brightness value of ~8 kHz/MOL.

[Place figure 7 here]

FIGURE AND TABLE LEGENDS:

Figure 1. Experimental workflow and schematic representation of scanning fluorescence cross-correlation spectroscopy and cross-correlation number and brightness analysis at cell-cell contacts. (**A**) Scheme of sample preparation: Two cell populations transfected with the protein of interest (*e.g.,* APLP1) fused to two spectrally distinct fluorescent proteins (*e.g.,* mEYFP and mCardinal) are mixed after transfection. Contacts of differently transfected cells are selected in the microscopy experiments. To avoid interference with extracellular binding domains, the fluorescent protein should be fused to the intracellular terminus of the protein of interest. (**B**) Scanning FCCS (sFCCS) measurements are performed perpendicular to the cell-cell contact in two spectral channels (channel 1, green and channel 2, red). Scan lines (represented as kymographs) are aligned and membrane pixels summed. Then, ACFs and CCFs are calculated from the intensity traces $F_i(t)$. ACFs are represented in red and green. CCF is represented in blue. (**C**) Cross-correlation N&B (ccN&B) acquisition results in a three-dimensional (x-y-time) image stack. A ROI is selected around the cell-cell contact. Then channel and cross-correlation brightness (ε_1, ε_2, and B_{cc}) values are calculated in each cell-cell contact pixel. The results are then visualized as histograms, pooling all selected pixels.

Figure 2. Scanning fluorescence cross-correlation spectroscopy control measurements. (**A**) Representative images of mixed HEK 293T cells expressing myr-palm-mEYFP/-mCardinal as negative control for *trans* interactions. The yellow arrow indicates the sFCCS scan path. Scale bars are 5 µm. (**B**) Representative images of HEK 293T cells expressing myr-palm-mCardinal-mEYFP hetero-dimer (left: green channel, right: red channel) as positive cross-correlation control. The yellow arrow indicates the sFCCS scan path. Scale bars are 5 µm. (**C**) Representative CFs (green: ACF in green channel (mEYFP), red: ACF in red channel (mCardinal), blue: CCF) obtained in sFCCS measurements for negative control. Solid lines show fits of a two-dimensional diffusion model to the CFs. (**D**) Representative CFs (green: ACF in green channel (mEYFP), red: ACF in red channel (mCardinal), blue: CCF) obtained in sFCCS measurement of the positive control. Solid lines show fits of a two-dimensional diffusion model to the CFs.

Figure 3. Scanning fluorescence cross-correlation spectroscopy measurements of APLP1 interactions at cell-cell contacts. (**A**, **B**) Representative images of HEK 293T cells expressing APLP1-mEYFP (green)/ APLP1-mCardinal (red) before (**A**) and 30 min after zinc ion treatment (**B**,

different cells). The yellow arrows indicate the sFCCS scan path. Scale bars are 5 µm. (**C**, **D**) Representative CFs (green: ACFs in green channel (mEYFP), red: ACFs in red channel (mCardinal), blue: CCFs) obtained in sFCCS measurements for (**C**) APLP1 before zinc ion treatment and (**D**) after zinc ion treatment. Solid lines show fits of a two-dimensional diffusion model to the CFs. (**E**) Box plots of relative cross-correlation obtained from sFCCS analysis of negative control ("negative"), APLP1 in absence and presence of zinc ions, and positive cross-correlation control ("positive"). Plots show median values and whiskers ranging from minimum to maximum values. (**F**) Box plots of normalized molecular brightness in green channel (mEYFP) obtained from sFCCS analysis of APLP1 at cell-cell contacts in the absence and presence of zinc ions. Brightness values were corrected for non-fluorescent mEYFP based on sFCS measurements of myr-palm-mEYFP-mEYFP homo-dimers expressed in HEK 293T cells, measured under the same conditions[23]. Plots show median values and whiskers ranging from minimum to maximum values.

Figure 4. Segment-wise analysis of scanning fluorescence cross-correlation spectroscopy measurements of negative cross-correlation control. (**A**) Fluorescence intensity in green (F_1) and red channel (F_2) of two different time segments (each measurement was analyzed in 20 segments of ~20 s each), obtained from sFCCS measurement of negative control. (**B**) CCFs of each of the 20 segments. The CCFs for segments 1 and 2 are highlighted in red and orange, respectively. (**C**, **D**) ACFs of each segment in green (**C**) and red (**D**) channel. The ACFs for segments 1 and 2 are highlighted in red and orange, respectively.

Figure 5. Perturbations in scanning fluorescence cross-correlation spectroscopy measurements at cell-cell contacts, exemplified for negative cross-correlation control. (**A**) Full fluorescence time series for an exemplar measurement in green (F_1) and red channel (F_2). The solid red lines represent a double-exponential fit of the time series in each channel. (**B**, **C**) CFs (green: ACFs in green channel, red: ACFs in red channel, blue: CCFs) of the fluorescence time series shown in **A**, calculated by (**B**) correlating the whole measurement or (**C**) correlating 20 segments separately and averaging the least distorted CFs of ~80% (green channel) and ~50% (red channel) of the segments. Solid lines represent fit of a two-dimensional diffusion model to the data. (**D**) Full fluorescence time series and double-exponential fit (solid red lines) of measurement characterized by substantial bleaching in green (F_1) and red channel (F_2). (**E**, **F**) CFs (green: ACFs in green channel, red: ACFs in red channel, blue: CCFs) of the fluorescence time series shown in **D**, calculated by (**E**) correlating the whole measurement or (**F**) applying the bleaching correction, Equation 1, correlating 20 segments separately and averaging the least distorted CFs of ~90% (both channels) of the segments. Solid lines represent fit of a two-dimensional diffusion model to the data.

Figure 6. Cross-correlation Number and Brightness measurements of APLP1 interactions at cell-cell contacts. (**A**–**C**) Representative ccN&B image frames of cell-cell contacts between APLP1-mEYFP and APLP1-mCardinal expressing HEK 293T cells without (**A**) and with zinc ions (**B**) or myr-palm-mEYFP and myr-palm-mCardinal expressing cells as negative cross-correlation control (**C**). Scale bars are 5 µm. (**D**–**F**) Cross-correlation brightness (B_{cc}) histograms of all examined pixels and cells obtained from ccN&B analysis of cell–cell contacts in APLP1 samples (**D**), zinc-treated APLP1 samples (**E**) and samples containing myr-palm-mEYFP and myr-palm-mCardinal (**F**). (**G**, **H**)

Normalized brightness histograms of APLP1 samples (**G**: without zinc ions, **H**: with zinc ions) for the green channel (mEYFP) obtained from brightness analysis of the same cells and ROIs used for the calculation of B_{cc}. Inset in G shows a magnification in the normalized brightness range of -2 to 10. Brightness values were corrected for non-fluorescent mEYFP based on N&B measurements of myr-palm-mEYFP-mEYFP homo-dimers expressed in HEK 293T cells, measured under the same conditions[23].

Figure 7. Detector calibration for Number and Brightness analysis. (**A**) Representative image from N&B measurements of HEK 293T cells expressing GPI-mCherry. A ROI (blue dashed rectangle) was selected in the background. (**B**) Pixel brightness histogram of all pixels corresponding to the ROI shown in **A**. The average pixel brightness, obtained from fitting the pixel brightness histogram with a Gaussian function, is ~0.1 cts./(MOL·dwell time). Data were acquired at 25 µs pixel dwell time. (**C**) Molecular brightness obtained from N&B analysis of GPI-mCherry expressed in HEK 293T cells, measured at three different laser powers (6 cells each, 561 nm excitation, 25 µs pixel dwell time). Data are displayed as mean $\pm$ SD. A linear regression (red line) provides an offset value of 0.11 $\pm$ 0.02 cts./(MOL·dwell time). (**D**) Plot of pixel variance as a function of pixel intensity from N&B measurements of a dried solution of a fluorescent dye (excited at 561 nm), pooled from all pixels of multiple measurements in different regions of the sample. The solid red line shows a linear fit of the data, resulting in a slope of 1.1, providing the S factor of the detector calibration. (**E**) Molecular brightness as a function of detector count rate, obtained from N&B measurements of diluted fluorophore solutions (excited at 488 nm). A previously published correction scheme[38] was applied using different possible values for the detector dead time.

DISCUSSION:

The experimental procedure described here allows the investigation of protein-protein *trans* interactions at cell-cell contacts, employing fluorescence fluctuation spectroscopy techniques, namely sFCCS and ccN&B. These methods involve a statistical analysis of fluorescence fluctuations emitted by two spectrally separated FPs fused to the protein(s) of interest at a contact of two neighboring cells, each expressing one or the other fusion protein. The presence of *trans* complexes is quantified by probing the degree of co-diffusion of proteins in neighboring PMs. In addition to detailed protocols on sample preparation, data acquisition and analysis, this article provides experimental evidence of the successful application of the assay on the neuronal adhesion protein APLP1. We show that APLP1 undergoes specific, homotypic *trans* interactions at cell-cell contacts. Further, zinc ions promote the formation of APLP1 clusters at cell-cell contacts that provide a multivalent platform for *trans* interactions and, thus, induce enhanced *trans* binding.

In contrast to previous assays to detect such interactions based on disruptive biochemical methods[6], the presented approach can be performed directly on living cells, with no need for fixation or isolation of protein complexes. Moreover, it provides molecular specificity and information by detection of fluorescent proteins genetically fused to the protein of interest, in contrast to previous qualitative assays[8, 9]. Differently from other fluorescence based approaches such as FRET[10] and fluorescence complementation[11], there is no requirement for the fluorescent

labels to be localized on the extracellular side (potentially interfering with protein-protein interactions). Nevertheless, it has to be noted that C-terminal FPs might still alter the binding to intracellular components, *e.g.,* adaptor proteins that mediate interactions with the cytoskeleton. Notably, the assay is applicable to both homo- and heterotypic interactions.

A few requirements for a successful application of the presented assay are worth mentioning. The performed fluorescence fluctuation methods are based on temporal measurements that require bright and photostable monomeric FPs, which is a major constraint for many red FPs[23]. Even though the presented scanning scheme is particularly well suited for the investigation of the slow dynamics of transmembrane proteins, which are typically involved in cell-cell interactions, residual photobleaching may still occur. Therefore, we present a detailed description of correction schemes, *i.e.* a bleaching correction for sFCCS and boxcar filter for ccN&B, which minimize such perturbations. Further, we discuss numerical alignment algorithms that effectively correct for other systematic perturbations, such as lateral movement of cells, and provide guidelines to remove transient instabilities. A major source of such instabilities is vesicular transport, *i.e.,* intracellular vesicles carrying the protein of interest that transiently enter the focal volume. Although varying from case to case, this phenomenon can in general severely disturb data acquisition and analysis. However, the application of correction algorithms improves the stability of the acquisition, allowing extended measurement times that are needed to probe the especially slow diffusive dynamics. In this regard, it has to be underlined that the presence of diffusive dynamics is an essential condition for the method to work. The example of zinc ion mediated APLP1 clustering shows a drastic example of large, very slow protein complexes ($D \approx 0.001\ \mu m^2/s$) that push the technique to its limits and prevent an accurate quantification of the underlying dynamics, due to large noise induced by the limited acquisition time[30, 17].

In this context, recent advances on combing sFCS and super-resolution approaches, *e.g.,* scanning stimulated emission depletion FCS (STED-FCS), may be beneficial by providing a smaller focal volume and thus smaller effective diffusion times[39, 40]. This could also help to resolve protein clusters in case of an inhomogeneous localization of the protein of interest at the cell-cell contact, as observed for APLP1 in the presence of zinc. Unfortunately, a cross-correlation implementation of scanning STED-FCS, *i.e.,* STED-FCCS, that could be directly applied here, has not been successfully demonstrated yet due to the difficulty of finding compatible dyes for two-color STED-FCS. In the case of sufficiently fast dynamics ($D \geq$ ~$0.05\ \mu m^2/s$), sFCCS analysis allows to quantify the diffusion of proteins at cell-cell contacts or in other regions of the PM[12].

Further, a brightness analysis can be performed of all data (sFCCS and ccN&B), providing an estimate of the stoichiometry of *trans* protein complexes. It should be mentioned that the accuracy of the stoichiometry quantification increases with the amount of proteins that bind in *trans* (*i.e.,* if there are only few *cis* complexes which could also affect the brightness determination). Brightness analysis does not allow resolving mixtures of different oligomeric states, *e.g., cis* monomers and *trans* tetramers. More in general, it should be noted that N&B cannot resolve mixtures of different oligomeric species homogeneously distributed in a sample. If multiple species are present within a pixel, one single value of brightness will be measured (*i.e.,* a weighted average of the brightness of each oligomeric species). The statistical distribution of

the observed brightness values (*e.g.,* in different pixels) is not directly connected to the relative amounts of oligomeric species. To resolve such mixtures, other methods should be used (*e.g.,* spatial intensity distribution analysis (SpIDA)[41], photon counting histogram (PCH)[42]). Similarly, the quantification of the spectral cross-correlation in sFCCS provides an accurate quantification of the fraction of bound and unbound proteins only for simple, known stoichiometries, *e.g.,* 1:1. For a more complex stoichiometry, further assumptions have to be made[43]. Overall, brightness analysis remains a powerful experimental tool, if the detector system and the fraction of non-fluorescent FPs are calibrated[23] as described in the protocols.

Although the application presented here is focused on protein-protein interactions in adherent cells, the assay can be applied to a wider range of samples *e.g.,* suspension cells. For such systems, correction for lateral cell movement may be particularly crucial. In addition, it can be easily applied to model membrane systems such as GUVs or GPMVs, allowing the quantification of molecular interactions under well controlled conditions, *e.g.,* different lipid compositions or membranes lacking an organized cytoskeleton. When performing sFCCS on such vesicles, vertical motion may cause additional signal fluctuations, but can be minimized when focusing on large vesicles. In this context, multiple combinations are promising, *e.g.,* GUV-/ GPMV-cell mixing[12]. As shown in a recent publication, the formation of immune synapses can be successfully modeled by such systems[44]. Thus, the presented assay will certainly be useful for the investigation of a large variety of cell-cell interactions.

ACKNOWLEDGMENTS:

This work was partially supported by the Deutsche Forschungsgemeinschaft (DFG) grant 254850309. The authors thank Madlen Luckner for critical reading of the manuscript.

DISCLOSURES:

The authors have nothing to disclose.

REFERENCES:

1. Alberts, B., Johnson, A., Lewis, J., Raff, M., Roberts, K., Walter, P. *Molecular biology of the cell*. Garland Science. (2002).
2. Tepass, U., Truong, K., Godt, D., Ikura, M., Peifer, M. Cadherins in embryonic and neural morphogenesis. *Nature Reviews Molecular Cell Biology*. **1** (2), 91–100, doi: 10.1038/35040042 (2000).
3. Harris, T. J. C., Tepass, U. Adherens junctions: from molecules to morphogenesis. *Nature Reviews Molecular Cell Biology*. **11** (7), 502–514, doi: 10.1038/nrm2927 (2010).
4. Hernández, J. M., Podbilewicz, B. The hallmarks of cell-cell fusion. *Development (Cambridge, England)*. **144** (24), 4481–4495, doi: 10.1242/dev.155523 (2017).
5. Huppa, J. B., Davis, M. M. T-cell-antigen recognition and the immunological synapse. *Nature Reviews Immunology*. **3** (12), 973–983, doi: 10.1038/nri1245 (2003).
6. Kaden, D., Voigt, P., Munter, L. -M., Bobowski, K. D., Schaefer, M., Multhaup, G. Subcellular localization and dimerization of APLP1 are strikingly different from APP and APLP2. *Journal of cell science*. **122** (Pt 3), 368–377, doi: 10.1242/jcs.034058 (2009).
7. Yap, A. S., Michael, M., Parton, R. G. Seeing and believing: recent advances in imaging

cell-cell interactions. *F1000Research*. **4** (F1000 Faculty Rev), 273, doi: 10.12688/f1000research.6435.1 (2015).
8. Kashef, J., Franz, C. M. Quantitative methods for analyzing cell–cell adhesion in development. *Developmental Biology*. **401** (1), 165–174, doi: 10.1016/J.YDBIO.2014.11.002 (2015).
9. Soba, P. *et al.* Homo- and heterodimerization of APP family members promotes intercellular adhesion. *The EMBO Journal*. **24** (20), 3624–3634, doi: 10.1038/sj.emboj.7600824 (2005).
10. Kim, S. A., Tai, C. -Y., Mok, L. -P., Mosser, E. A., Schuman, E. M. Calcium-dependent dynamics of cadherin interactions at cell-cell junctions. *Proceedings of the National Academy of Sciences of the United States of America*. **108** (24), 9857–62, doi: 10.1073/pnas.1019003108 (2011).
11. Feinberg, E. H. *et al.* GFP Reconstitution Across Synaptic Partners (GRASP) Defines Cell Contacts and Synapses in Living Nervous Systems. *Neuron*. **57** (3), 353–363, doi: 10.1016/J.NEURON.2007.11.030 (2008).
12. Dunsing, V., Mayer, M., Liebsch, F., Multhaup, G., Chiantia, S. Direct evidence of amyloid precursor-like protein 1transinteractions in cell-cell adhesion platforms investigated via fluorescence fluctuation spectroscopy. *Molecular biology of the cell*. **28** (25), 3609–3620, doi: 10.1091/mbc.E17-07-0459 (2017).
13. Schneider, F. *et al.* Diffusion of lipids and GPI-anchored proteins in actin-free plasma membrane vesicles measured by STED-FCS. *Molecular Biology of the Cell*. **28** (11), 1507–1518, doi: 10.1091/mbc.E16-07-0536 (2017).
14. Bacia, K., Kim, S. A., Schwille, P. Fluorescence cross-correlation spectroscopy in living cells. *Nature methods*. **3** (2), 83–89, doi: 10.1038/nmeth822 (2006).
15. Ries, J., Schwille, P. Studying Slow Membrane Dynamics with Continuous Wave Scanning Fluorescence Correlation Spectroscopy. *Biophysical Journal*. **91** (5), 1915–1924, doi: 10.1529/biophysj.106.082297 (2006).
16. Ries, J., Chiantia, S., Schwille, P. Accurate Determination of Membrane Dynamics with Line-Scan FCS. *Biophysical Journal*. **96** (5), 1999–2008, doi: 10.1016/j.bpj.2008.12.3888 (2009).
17. Chiantia, S., Ries, J., Schwille, P. Fluorescence correlation spectroscopy in membrane structure elucidation. *Biochimica et Biophysica Acta (BBA) - Biomembranes*. **1788** (1), 225–233, doi: 10.1016/J.BBAMEM.2008.08.013 (2009).
18. Digman, M. A., Dalal, R., Horwitz, A. F., Gratton, E. Mapping the number of molecules and brightness in the laser scanning microscope. *Biophysical journal*. **94** (6), 2320–2332, doi: 10.1529/biophysj.107.114645 (2008).
19. Dalal, R. B., Digman, M. A., Horwitz, A. F., Vetri, V., Gratton, E. Determination of particle number and brightness using a laser scanning confocal microscope operating in the analog mode. *Microscopy research and technique*. **71** (1), 69–81, doi: 10.1002/jemt.20526 (2008).
20. Unruh, J. R., Gratton, E. Analysis of Molecular Concentration and Brightness from Fluorescence Fluctuation Data with an Electron Multiplied CCD Camera. *Biophysical Journal*. **95** (11), 5385–5398, doi: 10.1529/biophysj.108.130310 (2008).
21. Digman, M. A., Wiseman, P. W., Choi, C., Horwitz, A.R., Gratton, E. Stoichiometry of

molecular complexes at adhesions in living cells. *Proceedings of the National Academy of Sciences of the United States of America*. **106** (7), 2170–2175, doi: 10.1073/pnas.0806036106 (2009).
22. Hellriegel, C., Caiolfa, V. R., Corti, V., Sidenius, N., Zamai, M. Number and brightness image analysis reveals ATF-induced dimerization kinetics of uPAR in the cell membrane. *The FASEB journal : official publication of the Federation of American Societies for Experimental Biology*. **25** (9), 2883–2897, doi: 10.1096/fj.11-181537 (2011).
23. Dunsing, V., Luckner, M., Zühlke, B., Petazzi, R. A., Herrmann, A., Chiantia, S. Optimal fluorescent protein tags for quantifying protein oligomerization in living cells. *Scientific Reports*. **8** (1), 10634, doi: 10.1038/s41598-018-28858-0 (2018).
24. Chen, Y., Johnson, J., Macdonald, P., Wu, B., Mueller, J. D. Observing Protein Interactions and Their Stoichiometry in Living Cells by Brightness Analysis of Fluorescence Fluctuation Experiments. *Methods in enzymology*. **472**, 345–363, doi: 10.1016/S0076-6879(10)72026-7 (2010).
25. Kapusta, P. Absolute Diffusion Coefficients: Compilation of Reference Data for FCS Calibration. at <https://www.picoquant.com/images/uploads/page/files/7353/appnote_diffusioncoefficients.pdf> (2010).
26. Foo, Y. H., Naredi-Rainer, N., Lamb, D. C., Ahmed, S., Wohland, T. Factors affecting the quantification of biomolecular interactions by fluorescence cross-correlation spectroscopy. *Biophysical journal*. **102** (5), 1174–83, doi: 10.1016/j.bpj.2012.01.040 (2012).
27. Baum, M., Erdel, F., Wachsmuth, M., Rippe, K. Retrieving the intracellular topology from multi-scale protein mobility mapping in living cells. *Nature Communications*. **5**, 4494, doi: 10.1038/ncomms5494 (2014).
28. Wohland, T., Rigler, R., Vogel, H. The standard deviation in fluorescence correlation spectroscopy. *Biophysical journal*. **80** (6), 2987–99, doi: 10.1016/S0006-3495(01)76264-9 (2001).
29. Ries, J. *et al.* Automated suppression of sample-related artifacts in Fluorescence Correlation Spectroscopy. *Optics Express*. **18** (11), 11073, doi: 10.1364/OE.18.011073 (2010).
30. Ries, J., Schwille, P. New concepts for fluorescence correlation spectroscopy on membranes. *Physical Chemistry Chemical Physics*. **10** (24), 3487, doi: 10.1039/b718132a (2008).
31. Mayer, M. C. *et al.* Amyloid precursor-like protein 1 (APLP1) exhibits stronger zinc-dependent neuronal adhesion than amyloid precursor protein and APLP2. *Journal of Neurochemistry*. **137** (2), 266–276, doi: 10.1111/jnc.13540 (2016).
32. Linkert, M. *et al.* Metadata matters: access to image data in the real world. *The Journal of Cell Biology*. **189** (5), 777–782, doi: 10.1083/jcb.201004104 (2010).
33. Trullo, A., Corti, V., Arza, E., Caiolfa, V. R., Zamai, M. Application limits and data correction in number of molecules and brightness analysis. *Microscopy Research and Technique*. **76** (11), 1135–1146, doi: 10.1002/jemt.22277 (2013).
34. Nolan, R. *et al.* nandb-number and brightness in R with a novel automatic detrending algorithm. *Bioinformatics (Oxford, England)*. **33** (21), 3508–3510, doi:

10.1093/bioinformatics/btx434 (2017).
35. Hammond, G. R. V, Sim, Y., Lagnado, L., Irvine, R. F. Reversible binding and rapid diffusion of proteins in complex with inositol lipids serves to coordinate free movement with spatial information. *The Journal of cell biology*. **184** (2), 297–308, doi: 10.1083/jcb.200809073 (2009).
36. Hendrix, J., Dekens, T., Schrimpf, W., Lamb, D. C. Arbitrary-Region Raster Image Correlation Spectroscopy. *Biophysical journal*. **111** (8), 1785–1796, doi: 10.1016/j.bpj.2016.09.012 (2016).
37. Hendrix, J. *et al.* Live-cell observation of cytosolic HIV-1 assembly onset reveals RNA-interacting Gag oligomers. *The Journal of cell biology*. **210** (4), 629–46, doi: 10.1083/jcb.201504006 (2015).
38. Hendrix, J., Schrimpf, W., Höller, M., Lamb, D. C. Pulsed Interleaved Excitation Fluctuation Imaging. *Biophysical Journal*. **105** (4), 848–861, doi: 10.1016/J.BPJ.2013.05.059 (2013).
39. Honigmann, A. *et al.* Scanning STED-FCS reveals spatiotemporal heterogeneity of lipid interaction in the plasma membrane of living cells. *Nature Communications*. **5** (1), 5412, doi: 10.1038/ncomms6412 (2014).
40. Chojnacki, J. *et al.* Envelope glycoprotein mobility on HIV-1 particles depends on the virus maturation state. *Nature Communications*. **8** (1), 545, doi: 10.1038/s41467-017-00515-6 (2017).
41. Godin, A. G. *et al.* Revealing protein oligomerization and densities in situ using spatial intensity distribution analysis. *Proceedings of the National Academy of Sciences of the United States of America*. **108** (17), 7010–5, doi: 10.1073/pnas.1018658108 (2011).
42. Müller, J. D., Chen, Y., Gratton, E. Resolving Heterogeneity on the Single Molecular Level with the Photon-Counting Histogram. *Biophysical Journal*. **78** (1), 474–486, doi: 10.1016/S0006-3495(00)76610-0 (2000).
43. Kim, S. A., Heinze, K. G., Bacia, K., Waxham, M. N., Schwille, P. Two-Photon Cross-Correlation Analysis of Intracellular Reactions with Variable Stoichiometry. *Biophysical Journal*. **88** (6), 4319–4336, doi: 10.1529/BIOPHYSJ.104.055319 (2005).
44. Jenkins, E. *et al.* Reconstitution of immune cell interactions in free-standing membranes. *bioRxiv*. 311399, doi: 10.1101/311399 (2018).

Figure 1

Click here to access/download;Figure;figure1.pdf

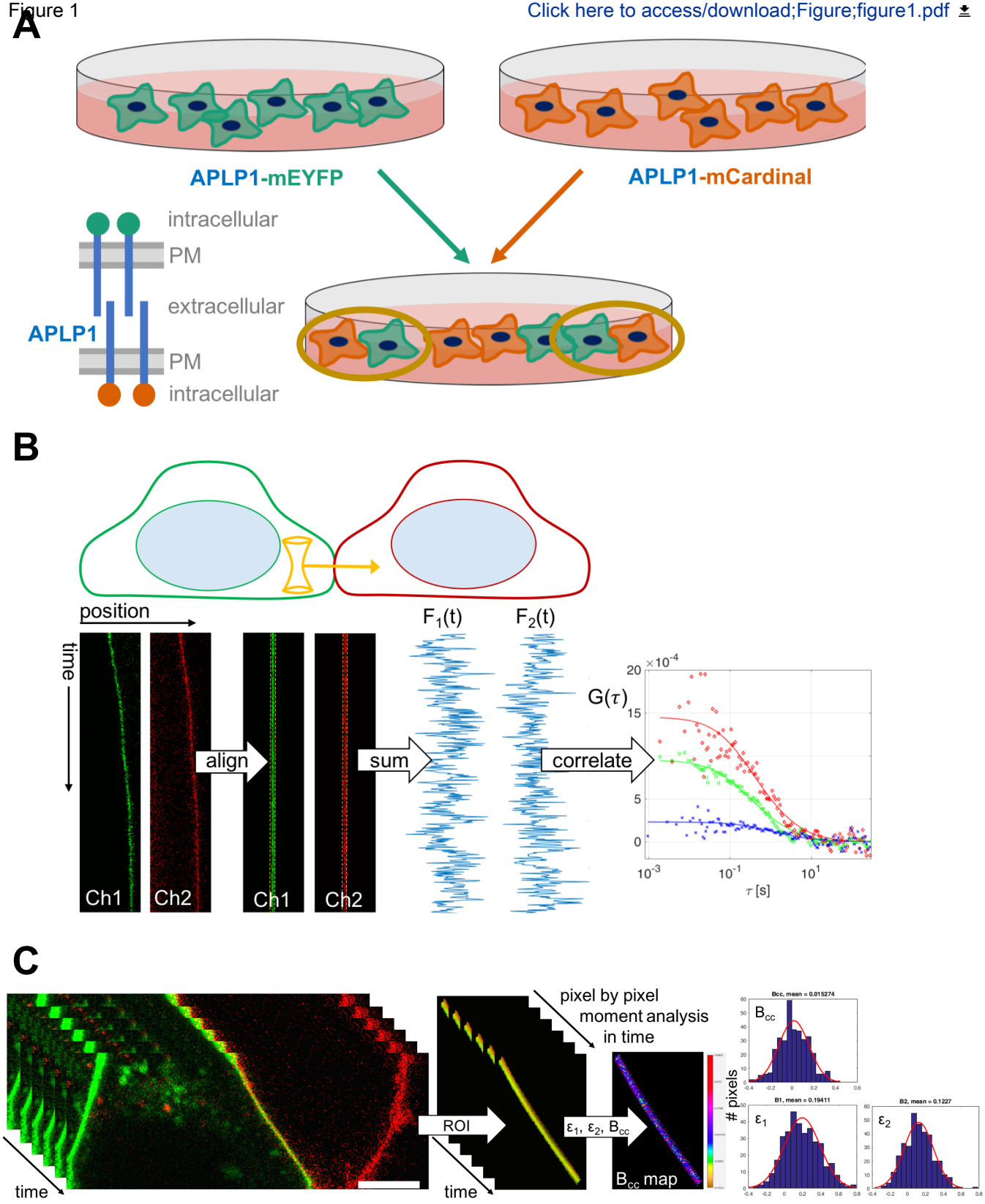

Figure 2

Click here to access/download;Figure;figure2.pdf

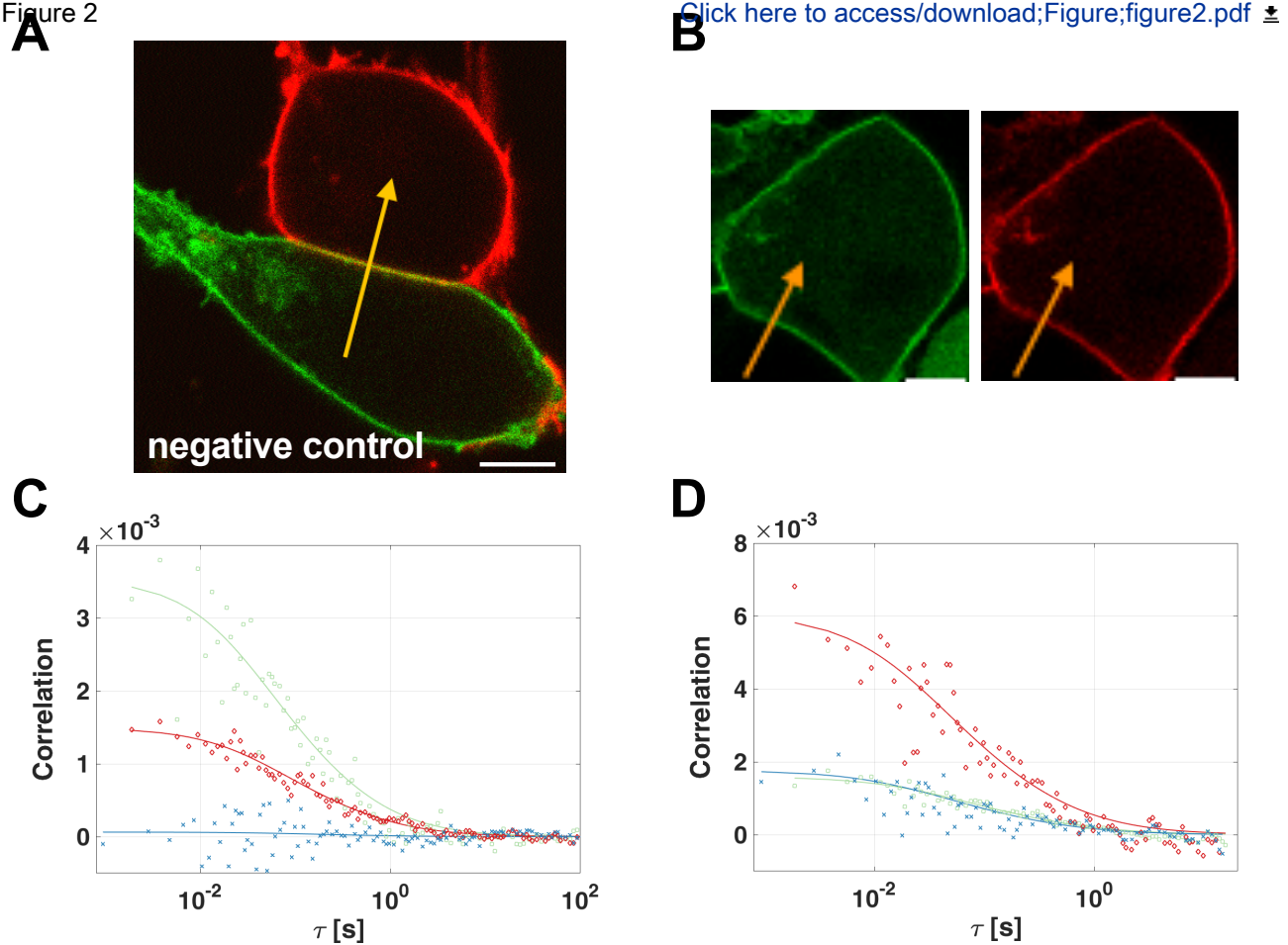

Figure 3

Click here to access/download;Figure;figure3.pdf

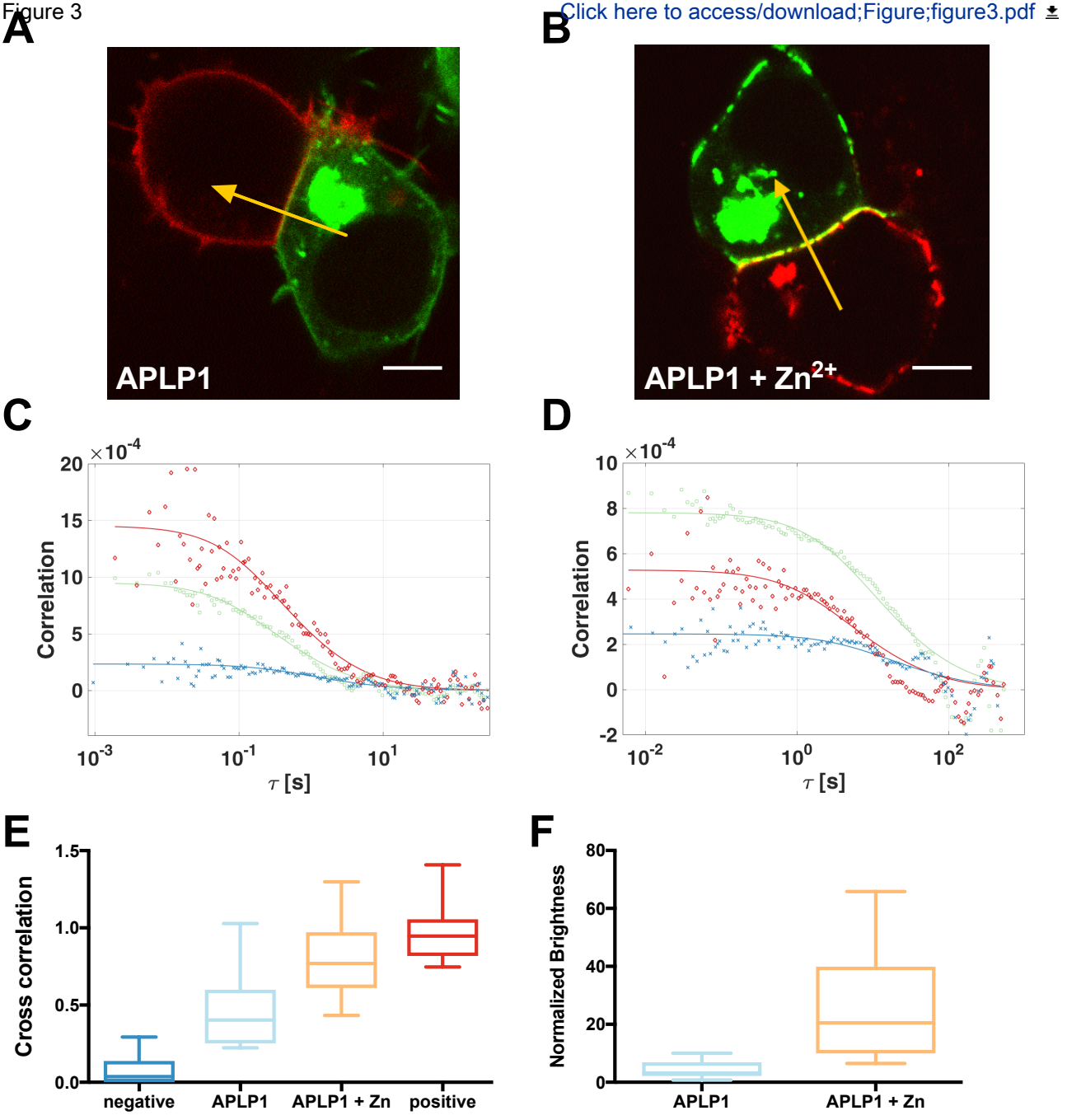

Figure 4

Click here to access/download;Figure;figure4.pdf

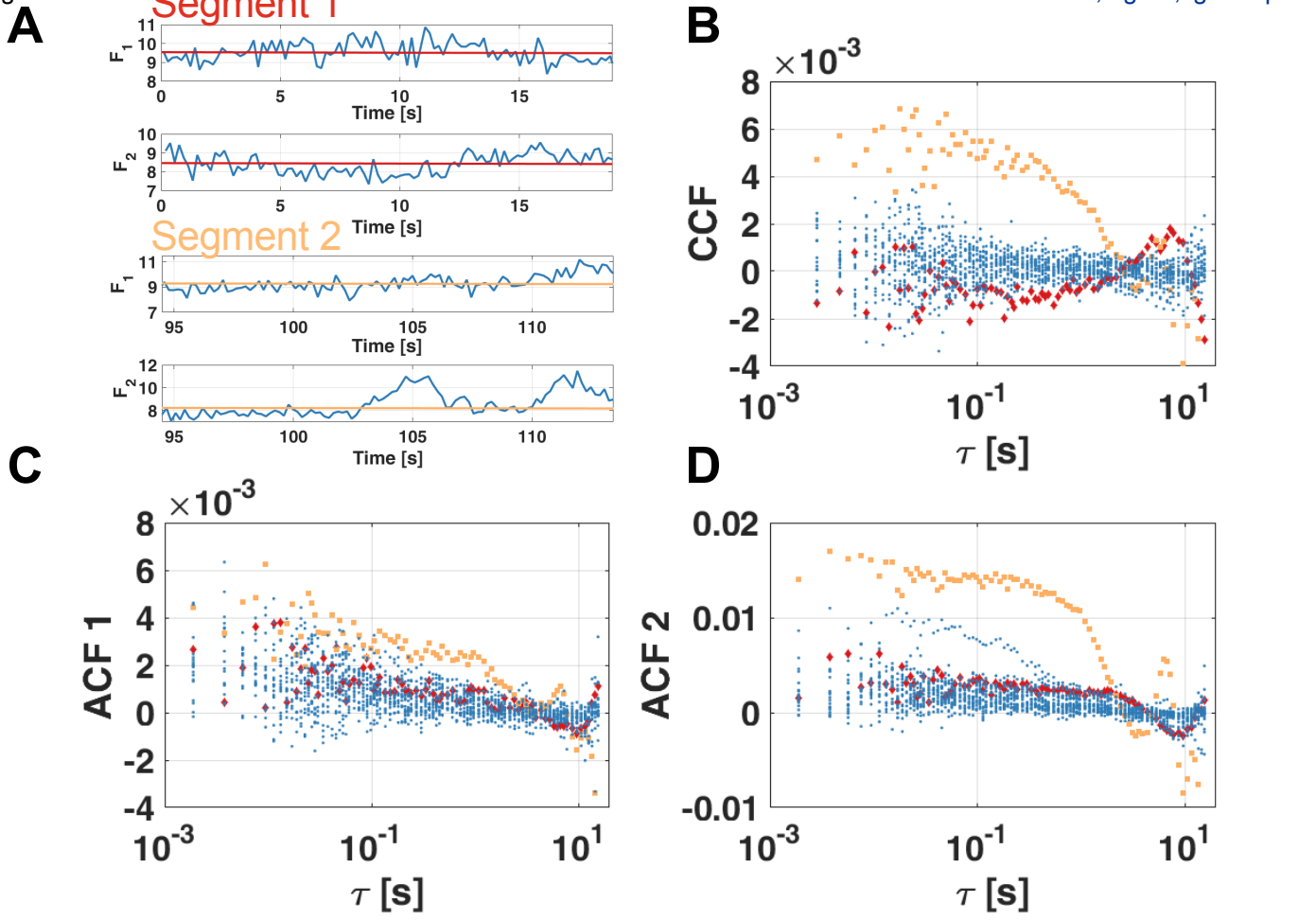

Figure 5

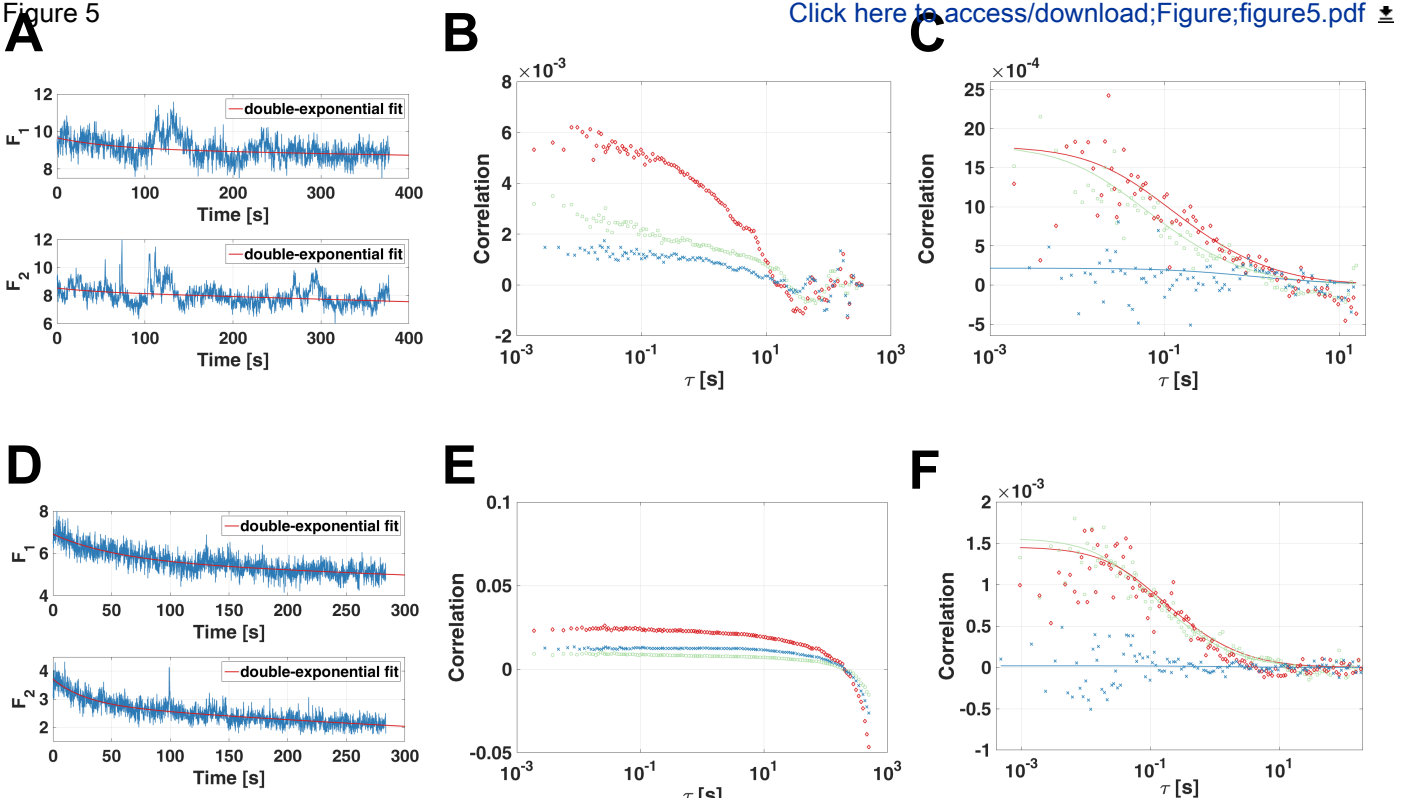

Figure 6

Click here to access/download;Figure;figure6.pdf

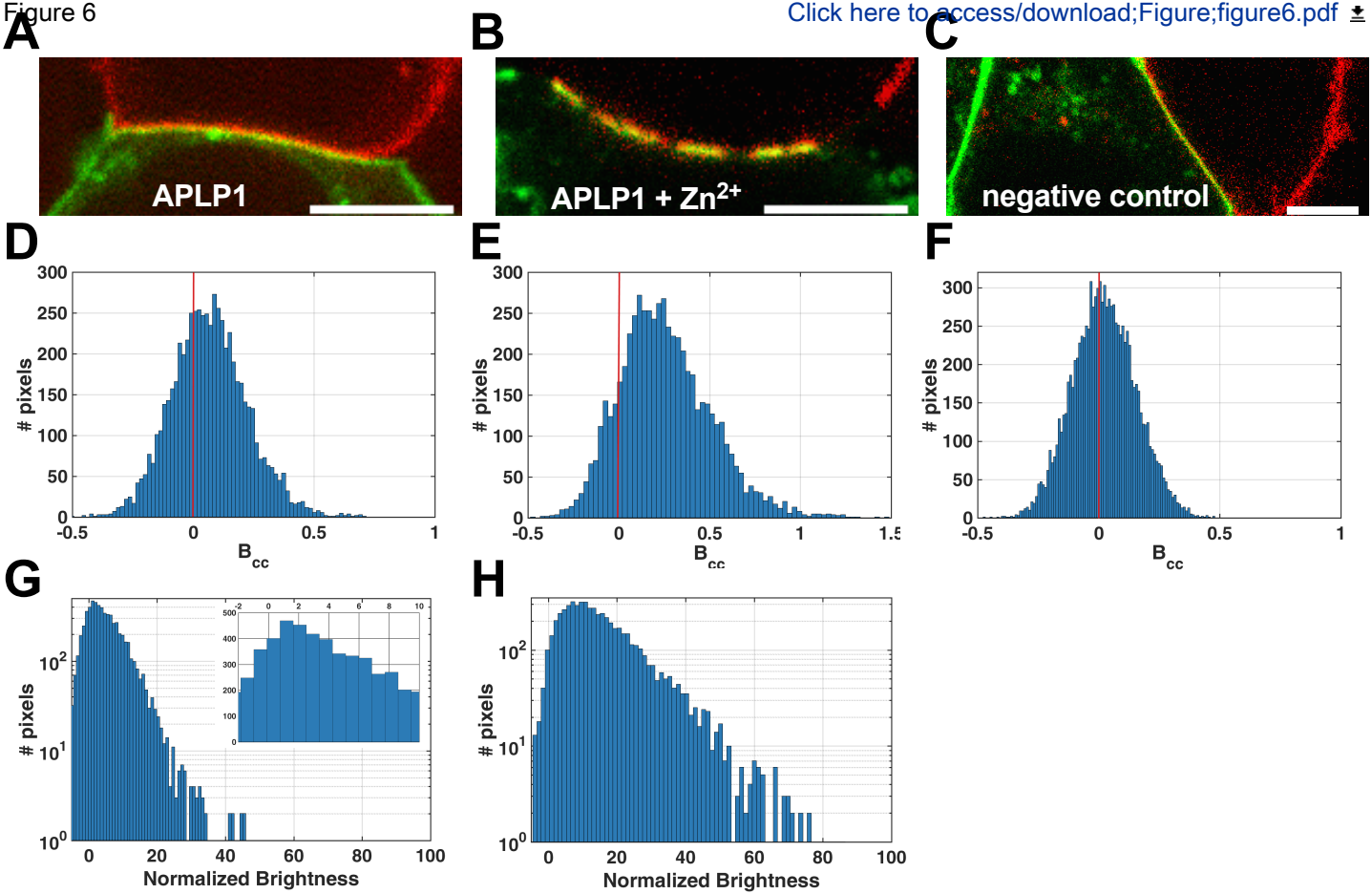

Figure 7

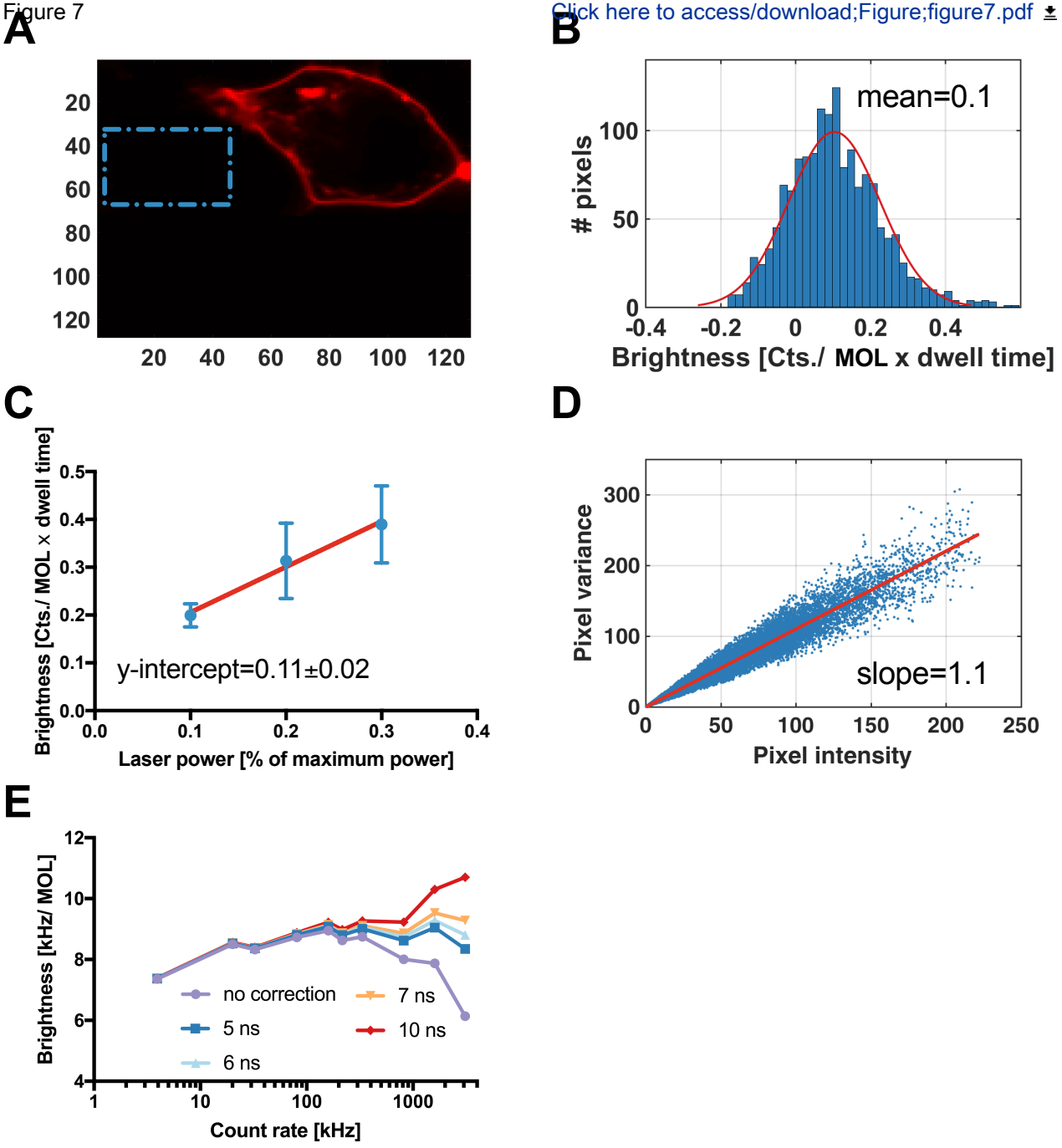

Table of Materials

Name of Material/ Equipment	Company	Catalog Number	Comments/Description
DMEM growth medium	PAN-Biotech	P04-01548	
DPBS w/o: Ca2+ and Mg2+	PAN-Biotech	P04-36500	
DPBS w: Ca2+ and Mg2+	PAN-Biotech	P04-35500	
Trypsin EDTA	PAN-Biotech	P10-023100	
TurboFect Transfection Reagent	Thermo Fisher Scientific	R0531	
HEK 293T cells	DSMZ	ACC 635	
Alexa Fluor 488 NHS Ester	Thermo Fisher Scientific	A20000	
Rhodamine B	Sigma-Alderich	83689-1G	
Plasmid DNA	Addgene	NA	See reference 12 (Dunsing et. al., MBoC 2017),for a detailed description of all p
6-well plate	Starlab	CC7672-7506	
35-mm glass bottom dishes	CellVis	D35-14-1.5-N	
Zeiss LSM780 confocal	Carl Zeiss	*NA*	
MATLAB software package	MathWorks	2015b	
Neubauer cell counting chamber	Marienfeld	640110	

ɔlasmids

jove JOURNAL OF VISUALIZED EXPERIMENTS
1 Alewife Center #200
Cambridge, MA 02140
tel. 617.945.9051
www.jove.com

ARTICLE AND VIDEO LICENSE AGREEMENT

Title of Article: A fluorescence fluctuation spectroscopy assay of protein-protein interactions at cell-cell contact

Author(s): Valentin Dunsing, Salvatore Chiantia

Item 1 (check one box): The Author elects to have the Materials be made available (as described at http://www.jove.com/author) via: [X] Standard Access [ ] Open Access

Item 2 (check one box):

[X] The Author is NOT a United States government employee.

[ ] The Author is a United States government employee and the Materials were prepared in the course of his or her duties as a United States government employee.

[ ] The Author is a United States government employee but the Materials were NOT prepared in the course of his or her duties as a United States government employee.

ARTICLE AND VIDEO LICENSE AGREEMENT

1. Defined Terms. As used in this Article and Video License Agreement, the following terms shall have the following meanings: "**Agreement**" means this Article and Video License Agreement; "**Article**" means the article specified on the last page of this Agreement, including any associated materials such as texts, figures, tables, artwork, abstracts, or summaries contained therein; "**Author**" means the author who is a signatory to this Agreement; "**Collective Work**" means a work, such as a periodical issue, anthology or encyclopedia, in which the Materials in their entirety in unmodified form, along with a number of other contributions, constituting separate and independent works in themselves, are assembled into a collective whole; "**CRC License**" means the Creative Commons Attribution-Non Commercial-No Derivs 3.0 Unported Agreement, the terms and conditions of which can be found at: http://creativecommons.org/licenses/by-nc-nd/3.0/legalcode; "**Derivative Work**" means a work based upon the Materials or upon the Materials and other pre-existing works, such as a translation, musical arrangement, dramatization, fictionalization, motion picture version, sound recording, art reproduction, abridgment, condensation, or any other form in which the Materials may be recast, transformed, or adapted; "**Institution**" means the institution, listed on the last page of this Agreement, by which the Author was employed at the time of the creation of the Materials; "**JoVE**" means MyJove Corporation, a Massachusetts corporation and the publisher of *The Journal of Visualized Experiments;* "**Materials**" means the Article and / or the Video; "**Parties**" means the Author and JoVE; "**Video**" means any video(s) made by the Author, alone or in conjunction with any other parties, or by JoVE or its affiliates or agents, individually or in collaboration with the Author or any other parties, incorporating all or any portion of the Article, and in which the Author may or may not appear.

2. Background. The Author, who is the author of the Article, in order to ensure the dissemination and protection of the Article, desires to have the JoVE publish the Article and create and transmit videos based on the Article. In furtherance of such goals, the Parties desire to memorialize in this Agreement the respective rights of each Party in and to the Article and the Video.

3. Grant of Rights in Article. In consideration of JoVE agreeing to publish the Article, the Author hereby grants to JoVE, subject to **Sections 4** and **7** below, the exclusive, royalty-free, perpetual (for the full term of copyright in the Article, including any extensions thereto) license (a) to publish, reproduce, distribute, display and store the Article in all forms, formats and media whether now known or hereafter developed (including without limitation in print, digital and electronic form) throughout the world, (b) to translate the Article into other languages, create adaptations, summaries or extracts of the Article or other Derivative Works (including, without limitation, the Video) or Collective Works based on all or any portion of the Article and exercise all of the rights set forth in (a) above in such translations, adaptations, summaries, extracts, Derivative Works or Collective Works and (c) to license others to do any or all of the above. The foregoing rights may be exercised in all media and formats, whether now known or hereafter devised, and include the right to make such modifications as are technically necessary to exercise the rights in other media and formats. If the "Open Access" box has been checked in **Item 1** above, JoVE and the Author hereby grant to the public all such rights in the Article as provided in, but subject to all limitations and requirements set forth in, the CRC License.

4. Retention of Rights in Article. Notwithstanding the exclusive license granted to JoVE in **Section 3** above, the Author shall, with respect to the Article, retain the non-exclusive right to use all or part of the Article for the non-commercial purpose of giving lectures, presentations or teaching classes, and to post a copy of the Article on the Institution's website or the Author's personal website, in each case provided that a link to the Article on the JoVE website is provided and notice of JoVE's copyright in the Article is included. All non-copyright intellectual property rights in and to the Article, such as patent rights, shall remain with the Author.

5. Grant of Rights in Video – Standard Access. This **Section 5** applies if the "Standard Access" box has been checked in **Item 1** above or if no box has been checked in **Item 1** above. In consideration of JoVE agreeing to produce, display or otherwise assist with the Video, the Author hereby acknowledges and agrees that, Subject to **Section 7** below, JoVE is and shall be the sole and exclusive owner of all rights of any nature, including, without limitation, all copyrights, in and to the Video. To the extent that, by law, the Author is deemed, now or at any time in the future, to have any rights of any nature in or to the Video, the Author hereby disclaims all such rights and transfers all such rights to JoVE.

6. Grant of Rights in Video – Open Access. This **Section 6** applies only if the "Open Access" box has been checked in **Item 1** above. In consideration of JoVE agreeing to produce, display or otherwise assist with the Video, the Author hereby grants to JoVE, subject to **Section 7** below, the exclusive, royalty-free, perpetual (for the full term of copyright in the Article, including any extensions thereto) license (a) to publish, reproduce, distribute, display and store the Video in all forms, formats and media whether now known or hereafter developed (including without limitation in print, digital and electronic form) throughout the world, (b) to translate the Video into other languages, create adaptations, summaries or extracts of the Video or other Derivative Works or Collective Works based on all or any portion of the Video and exercise all of the rights set forth in (a) above in such translations, adaptations, summaries, extracts, Derivative Works or Collective Works and (c) to license others to do any or all of the above. The foregoing rights may be exercised in all media and formats, whether now known or hereafter devised, and include the right to make such modifications as are technically necessary to exercise the rights in other media and formats. For any Video to which this Section 6 is applicable, JoVE and the Author hereby grant to the public all such rights in the Video as provided in, but subject to all limitations and requirements set forth in, the CRC License.

7. Government Employees. If the Author is a United States government employee and the Article was prepared in the course of his or her duties as a United States government employee, as indicated in **Item 2** above, and any of the licenses or grants granted by the Author hereunder exceed the scope of the 17 U.S.C. 403, then the rights granted hereunder shall be limited to the maximum rights permitted under such statute. In such case, all provisions contained herein that are not in conflict with such statute shall remain in full force and effect, and all provisions contained herein that do so conflict shall be deemed to be amended so as to provide to JoVE the maximum rights permissible within such statute.

8. Likeness, Privacy, Personality. The Author hereby grants JoVE the right to use the Author's name, voice, likeness, picture, photograph, image, biography and performance in any way, commercial or otherwise, in connection with the Materials and the sale, promotion and distribution thereof. The Author hereby waives any and all rights he or she may have, relating to his or her appearance in the Video or otherwise relating to the Materials, under all applicable privacy, likeness, personality or similar laws.

9. Author Warranties. The Author represents and warrants that the Article is original, that it has not been published, that the copyright interest is owned by the Author (or, if more than one author is listed at the beginning of this Agreement, by such authors collectively) and has not been assigned, licensed, or otherwise transferred to any other party. The Author represents and warrants that the author(s) listed at the top of this Agreement are the only authors of the Materials. If more than one author is listed at the top of this Agreement and if any such author has not entered into a separate Article and Video License Agreement with JoVE relating to the Materials, the Author represents and warrants that the Author has been authorized by each of the other such authors to execute this Agreement on his or her behalf and to bind him or her with respect to the terms of this Agreement as if each of them had been a party hereto as an Author. The Author warrants that the use, reproduction, distribution, public or private performance or display, and/or modification of all or any portion of the Materials does not and will not violate, infringe and/or misappropriate the patent, trademark, intellectual property or other rights of any third party. The Author represents and warrants that it has and will continue to comply with all government, institutional and other regulations, including, without limitation all institutional, laboratory, hospital, ethical, human and animal treatment, privacy, and all other rules, regulations, laws, procedures or guidelines, applicable to the Materials, and that all research involving human and animal subjects has been approved by the Author's relevant institutional review board.

10. JoVE Discretion. If the Author requests the assistance of JoVE in producing the Video in the Author's facility, the Author shall ensure that the presence of JoVE employees, agents or independent contractors is in accordance with the relevant regulations of the Author's institution. If more than one author is listed at the beginning of this Agreement, JoVE may, in its sole discretion, elect not take any action with respect to the Article until such time as it has received complete, executed Article and Video License Agreements from each such author. JoVE reserves the right, in its absolute and sole discretion and without giving any reason therefore, to accept or decline any work submitted to JoVE. JoVE and its employees, agents and independent contractors shall have

jove JOURNAL OF VISUALIZED EXPERIMENTS
1 Alewife Center #200
Cambridge, MA 02140
tel. 617.945.9051
www.jove.com

ARTICLE AND VIDEO LICENSE AGREEMENT

full, unfettered access to the facilities of the Author or of the Author's institution as necessary to make the Video, whether actually published or not. JoVE has sole discretion as to the method of making and publishing the Materials, including, without limitation, to all decisions regarding editing, lighting, filming, timing of publication, if any, length, quality, content and the like.

11. Indemnification. The Author agrees to indemnify JoVE and/or its successors and assigns from and against any and all claims, costs, and expenses, including attorney's fees, arising out of any breach of any warranty or other representations contained herein. The Author further agrees to indemnify and hold harmless JoVE from and against any and all claims, costs, and expenses, including attorney's fees, resulting from the breach by the Author of any representation or warranty contained herein or from allegations or instances of violation of intellectual property rights, damage to the Author's or the Author's institution's facilities, fraud, libel, defamation, research, equipment, experiments, property damage, personal injury, violations of institutional, laboratory, hospital, ethical, human and animal treatment, privacy or other rules, regulations, laws, procedures or guidelines, liabilities and other losses or damages related in any way to the submission of work to JoVE, making of videos by JoVE, or publication in *JoVE* or elsewhere by JoVE. The Author shall be responsible for, and shall hold JoVE harmless from, damages caused by lack of sterilization, lack of cleanliness or by contamination due to the making of a video by JoVE its employees, agents or independent contractors. All sterilization, cleanliness or decontamination procedures shall be solely the responsibility of the Author and shall be undertaken at the Author's expense. All indemnifications provided herein shall include JoVE's attorney's fees and costs related to said losses or damages. Such indemnification and holding harmless shall include such losses or damages incurred by, or in connection with, acts or omissions of JoVE, its employees, agents or independent contractors.

12. Fees. To cover the cost incurred for publication, JoVE must receive payment before production and publication the Materials. Payment is due in 21 days of invoice. Should the Materials not be published due to an editorial or production decision, these funds will be returned to the Author. Withdrawal by the Author of any submitted Materials after final peer review approval will result in a US$1,200 fee to cover pre-production expenses incurred by JoVE. If payment is not received by the completion of filming, production and publication of the Materials will be suspended until payment is received.

13. Transfer, Governing Law. This Agreement may be assigned by JoVE and shall inure to the benefits of any of JoVE's successors and assignees. This Agreement shall be governed and construed by the internal laws of the Commonwealth of Massachusetts without giving effect to any conflict of law provision thereunder. This Agreement may be executed in counterparts, each of which shall be deemed an original, but all of which together shall be deemed to me one and the same agreement. A signed copy of this Agreement delivered by facsimile, e-mail or other means of electronic transmission shall be deemed to have the same legal effect as delivery of an original signed copy of this Agreement.

A signed copy of this document must be sent with all new submissions. Only one Agreement required per submission.

CORRESPONDING AUTHOR:

Name:	SALVATORE CHIANTIA
Department:	BIOCHEMISTRY AND BIOLOGY
Institution:	POTSDAM UNIVERSITÄT
Article Title:	A fluorescence fluctuation spectroscopy assay for protein-protein interaction at cell-cell contacts
Signature:	Salvatore Chiantia
Date:	5.6.18

Please submit a signed and dated copy of this license by one of the following three methods:

1) Upload a scanned copy of the document as a pfd on the JoVE submission site;
2) Fax the document to +1.866.381.2236;
3) Mail the document to JoVE / Attn: JoVE Editorial / 1 Alewife Center #200 / Cambridge, MA 02139

For questions, please email submissions@jove.com or call +1.617.945.9051

Please note that all the editorial comments were addressed directly in the manuscript document.

Each comment has a corresponding answer in the form of a follow-up comment (visible as answer to the comment using Microsoft Office Word 2013 and newer versions).